國立交通大學
光電工程研究所
博士論文

硒化鎵晶體摻鉺特性及其應用在產生中紅外光源之研究

The Study of the Characteristics of Er:GaSe Crystal and Application to IR Source Generation

研究生：徐裕奎

指導教授：張振雄教授

中華民國 九十四年六月

硒化鎵晶體摻鉺特性及其應用在產生中紅外光源之研究

The Study of the Characteristics of Er:GaSe Crystal
and Application to IR Source Generation

研 究 生：徐裕奎　　　　　　　Student：Yu-Kuei Hsu

指導教授：張振雄 教授　　　　Advisor：Prof. Chen-Shiung Cheng

國立交通大學

光電工程研究所

博士論文

A dissertation
Submitted to Photonics & Institute of Electro-Optical Engineering
College of Electrical and Computer Science
National Chiao Tung University
in Partial Fulfillment of the Requirements
for the Degree of
Doctor of Philosophy
in
Electro-Optical Engineering
June 2005
Hsinchu, Taiwan, Republic of China

中華民國 九十四年六月

The Study of the Characteristics of Er:GaSe Crystal and Application to IR Source Generation

Student : Yu-Kuei Hsu   Advisor : Prof. Chen-Shiung Cheng

Department of Photonic & Institute of Electro-Optical Engineering
National Chiao Tung University

Abstract

In this dissertation, the centimeter size GaSe single crystals were grown by means of the non-stoichiometric mixture and quartz tube with a capillary. Good crystal quality was examined by X-ray rocking cure and EPMA measurements. The major studies are taken concern of the characteristics of Er-doped GaSe, because of an intra-$4f$ transition at a wavelength of 1.54 μm, which is important as a light source in optical communication technology. The optical properties of Er-doped GaSe crystals have been investigated by using temperature and power dependent photoluminescence, and Fourier-transform infrared spectrometer measurements. The new emission bands resulting from doping erbium and their transition mechanism were discussed. Additionally, the electrical characteristics and Er-related luminescence of Er-doped GaSe samples were also studied by means of Hall, DLTS, and IR photoluminescence measurements. The two impurity levels that act as radiative and nonradiative centers, respectively, were evaluated by DLTS and the temperature dependence of hole concentration measurements. Meanwhile, the possible origin of these impurity levels could be associated with the substitution of two Ga^{2+} atoms by one Er^{3+} atom or are related to a Ga vacancy via the interstratifying of an Er^{3+} ion at the interlayer site. The temperature-dependence of hole mobility was also analyzed by scattering from homopolar optical phonons and ionized impurities.

Besides, an optical parametric oscillator (OPO) based on periodically poled lithium niobate pumped by a Nd:YAG laser was demonstrated. Combined signal and idler pulse output from OPO with a maximum energy of 2.7 mJ, which corresponds to a slope efficiency of 25% have been achieved. The tuning range is 1.71 to 1.98 μm for

i

the signal wave and 2.81 to 2.30 μm for the idler wave. The signal and the idler waves are tuned and difference-frequency mixed in a GaSe crystal to produce tunable mid-IR from 4.35 to 14.25 μm. The DFG efficiency was less than the calculated value, mainly due to high reflection loss, poor surface quality, and OPO beam divergence. Additionally, we also demonstrated the infrared light source that provides picosecond pulses on microjoule energy level, widely tunable in the 2.4-30 μm wavelength range with pulse durations ~5 ps. The energies of several microjoule are obtained with a maximum of ~5 μJ at wavelength of 3.5 μm, corresponding to photon conversion efficiency of 8 %. The pump source is Nd:YAG laser at a wavelength of 1.064 μm and signal source is a parametric device based on a 10 Hz Nd:YAG amplifier system. This picosecond light source was applied to evaluate the nonlinear coefficient (d_{eff}) of crystals GaSe doped with erbium based on second harmonic generation. The variation in the d_{eff} values between undoped and erbium doped GaSe could be probably ascribed to the effect of erbium doping, which resulted in substitution or interstitial of Er atom in GaSe unit cell.

硒化鎵晶體摻鉺特性及其應用在產生中紅外光源之研究

研 究 生：徐裕奎　　　　　　　　　　　　　指導教授：張振雄 教授

國立交通大學 光電工程研究所

摘要

我們利用非等化學計量比的方法與改變石英甘鍋底部的形狀，成功成長了結晶性佳且大尺寸的硒化鎵單晶。此外，本文對於鉺元素摻雜於硒化鎵晶體的光學及電學性質也作了深入的探討，這是由於鉺元素所輻射出的 1.54μm 的波長，可作為光纖通訊中重要的光源。首先，利用改變光激發光功率及改變溫度的螢光光譜量測與室溫下紅外穿透光譜量測來檢測摻鉺硒化鎵的光學特性。從光學特性的分析中，鉺摻雜於硒化鎵晶體中除了會在高於價帶 64meV 處形成雜質能階外，也觀測到鉺元素本身所輻射的特徵光譜。在電性量測的實驗中，利用了變溫的霍爾效應實驗以及深層能階暫態光譜實驗來檢測摻鉺硒化鎵的電學特性。從分析中可得知，除了可以觀察到 64meV 淺的雜質能階外，還可以觀測到更深的 158meV 深層能階，我們也推測此深層能階扮演著硒化鎵晶體與鉺元素之間能量轉換的關鍵角色。除此之外，對於鉺元素在硒化鎵晶體中的取代機制以及電子在摻鉺後的硒化鎵晶體傳輸所受到的散色機制，也有更進一步的分析討論。

對於利用硒化鎵晶體應用在非線性光學之差頻效應來產生紅外光源的實驗，也是本文的另一個研究課題。我們分別利用兩種不同的雷射架構，成功的產生了奈秒及皮秒級脈衝式連續可調且具同調性的紅外光源，其所產生的光波範圍分別為 4.35-14.25 μm 及 2.4-30 μm。不同的脈衝時脈寬度的光源，會有其不同應用的領域。對於兩系統中所產生紅外光源的轉換效率，本文中也有深入的討論與分析。除此之外，利用二次諧波轉換效率的量測，可以定量獲得摻鉺硒化鎵晶體的二階非線性光學係數大於純的硒化鎵晶體的結果。推測二階非線性光學係數產生變化的原因，是由於鉺元素在硒化鎵晶體單層中以及層與層間發生取代行為，進而改變了原本的對稱性結構所致。
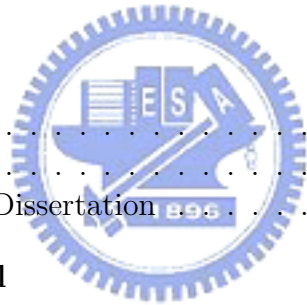
Acknowledgements

Table of Contents

List of Figures

List of Tables

Chapter 1

Introduction

1.1 Background

Gallium selenide (GaSe) is a native p-type semiconductor that belongs to the III-VI layered semiconductor family like GaS and InSe. Depending on the package type of separate layers and their amount in the unit cell, GaSe crystals can have a structure that corresponds to various polytype modifications. Four polytypes are known for GaSe(β, γ, δ and ε) and their polytypes of unit cell are shown in Fig. 1.1. A great deal of studies have made by several research groups to understand the polytypes in these compounds. The formation of a particular polytype or a mixture of several polytypes depends substantially on the growth method of single crystals. For example, the Czochralski and Bridgman-Stockbarger methods yield mainly the ε polytype. Gas transport reactions also yield the ε polytype with a large number of stacking faults. Needle crystals of γ, δ and ε polytypes are formed by vacuum sublimation. Single crystals of the β polytype are formed only occasionally. Most of the papers covered in this thesis deal with the ε type. Figure 1.2 shows structure of GaSe, and atomic configuration of GaSe layers. The main structural unit of GaSe is the elementary

1

layer with two molecules (four atoms) in the unit cell. The atoms are located in the planes normal to the C axis in the sequence Se-Ga-Ga-Se. Each GaSe layer thereby consists of two planes of Ga atoms, which are surrounded on two sides by the unit planes of the Se atoms. The location of atoms inside the layer corresponds to the D_{3h}^1 group of point symmetry. In this case, three anions form a tetrahedron along with the metal atom. The strong bonding between two sheets of the same layer is covalent with some ionic contribution. But the bonds between the complete four-fold layer is essentially of the Vander Waal type. Due to the characteristics of layer, GaSe exhibits a strongly pronounced structural anisotropy. Consequently, the ε type GaSe is a promising candidate material for nonlinear optical conversion devices in the near- to far-infrared wavelength(1-18μm), and the intermediate layer to connect such lattice-mismatched semiconductors as GaAs and Si with reduced number of misfit dislocations by the van der Waals epitaxy. Besides the removal of the constraint of the lattice mismatch, GaSe thin film possesses the advantages of stability against heating and oxidation under the ultra-high vaccum condition. GaSe has recently been reported to be applicable as a termination layer as well as an electronic passivation surface on Si even limited to nano-scaled structures.

Due to its relatively large band gap energy of 2.0 eV, impurity doping in GaSe has been investigated with much interest because of its possible applications for photo-electric devices in the visible region. The electric and optical properties of GaSe doped with elements of groups I, II, IV, and VII have been reported by many researchers. The hole concentration on the order of $10^{15} - 10^{16}\ cm^{-3}$ at room-temperature have been demonstrated by doping Cd[1], Zn[2], Cu[3], Mn[4], and Ag[5]. Activation energies for hole concentration are of the order of 300 meV for Cd, Zn, and Mn doped
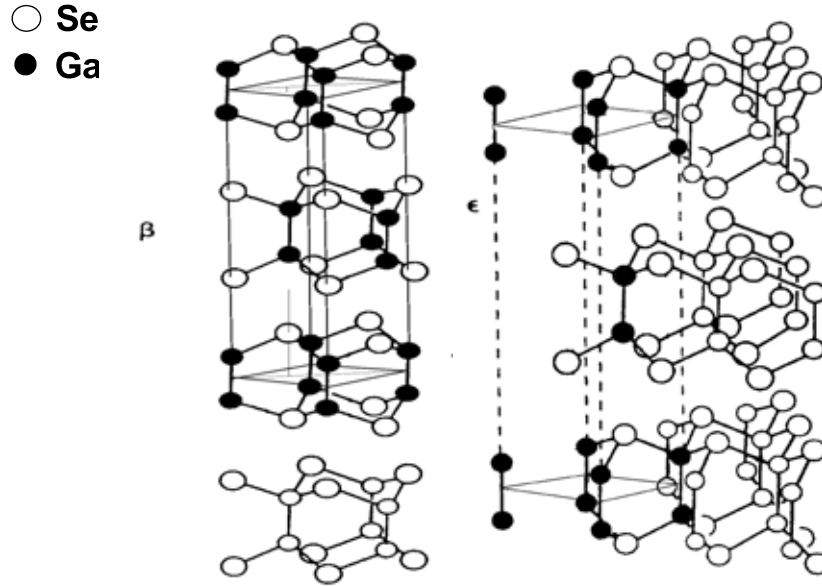
Figure 1.1: Polytypes of GaSe

GaSe, of the order 40 and 140 meV for Cu-doped samples, and of the order of 60 meV for Ag-doped samples. Until now only the dopants of Sn[6], Cl[7, 8] and I could act as donors in GaSe samples. The electron concentration for n-type GaSe are the order of $10^{12} - 10^{13}$ cm^{-3} at room-temperature. Attempts to get low resistivity n-type GaSe have been unsuccessful.

Except the above elements, much attention has been recently paid to GaSe doped with transition-metal elements and its optical properties. Trivalent rare-earth ions are well known for their special optical properties, which result from the factor that the electrons of the partially filled $4f$ shells are shielded from the surrounding completely filled $5s$ and $5p$ shells. The energy levels of the $4f$ shell have equal parity, and hence
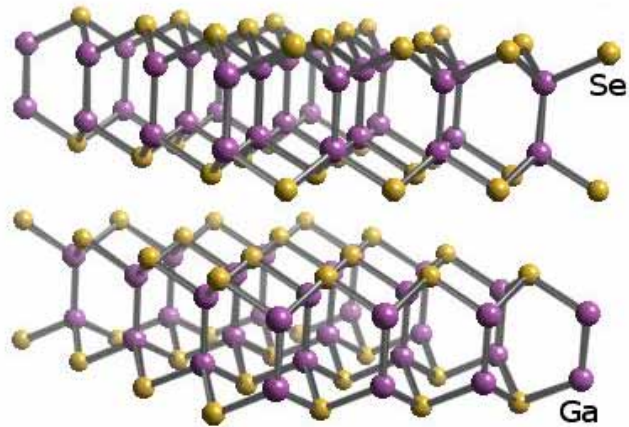
Figure 1.2: Layer structure of GaSe

electric dipole transitions are forbidden. In a solid, the slight mixing with odd-parity wavefunctions makes transition slightly allowed. The influence of the electric field around the ion removes the degeneracy of the $4f$-levels, resulting in a Stark-splitting of the energy levels. However, due to the shielding by the outer lying shells, the magnitude of the splitting is small, resulting in relative narrow emission lines, of which the wavelength is almost independent of the host material. The energy levels of the $4f$ shells arise from spin-spin and spin-orbit interactions and are often denoted using Russel-Saunders notation $^{2s+1}L_J$, in which S is the total spin angular momentum, L is the total orbital angular momentum quantum number and J is the magnitude of the total angular momentum, J=L+S according to vector model. There exist 14 rare-earth elements, that all have a different number of electrons in the incompletely filled $4f$ shells. As a result, each rare-earth ion has its own specific energy levels, and hence typical luminescence lines. The rare-earth ion erbium has transition at

4

1.54 μm, which is the standard wavelength used in optical telecommunication. The effect of doping with Gd[9], Yb[10], Dy[11], and Tm[12] on optical behaviors of GaSe crystals was studied.

GaSe possesses a number of exciting properties, which are listed in Table 1.1, for nonlinear optical application. Among these nonlinear optical crystals, GaSe has a transparency range extending from a wavelength of 0.65 to 18 μm where the optical absorption coefficient dose not exceed 1 cm^{-1} throughout the range. The ε type GaSe is a negative uniaxial crystal ($n_o > n_e$, where n_o and n_e denote the refractive indices in the ordinary and extraordinary direction). Its nonlinear optical coefficients are among the top five for birefringent crystal. Due to its large birefringence, it can satisfy phase matching (PM) conditions for optical configurations within the nonlinear optical crystals. Recently, incoherent parametric generation tunable in the range of 3.5-18 μm in GaSe (type-I PM) was obtained by using 110 ps pulses from actively mode-locked Er:YAG laser as a pump source[13]. Subsequently, picosecond pulses of mode-locked Er:Cr:YSGG laser were used to pump a traveling-wave optical parametric generation(OPG); type-I and type-II OPG provided continuous tunability in the range of 3.5-14 and 3.9-10 μm, respectively[14]. On the other hand, there have been a number of reports on difference frequency generation (DFG) to achieve tunable and coherent mid-IR for GaSe by using variety of laser sources.[15, 16] Additionally, few papers reported on THz-wave generation from GaSe.[17, 18, 19] Because GaSe has lowest absorption coefficients in the THz wavelength region. Consequently, GaSe has the largest figure of merit for the THz generation ($d_{eff}^2/n^3\alpha^2$), which is several orders of mabnitude larger than that for bulk LiNbO$_3$ at 300 μm. According to Y.J. Ding's results, an efficient and coherent THz wave tunable in the two extremely wide

Crystal	Nonlinear Coefficient (pm/V)	Merit Factor d^2/n^3	Transparency Range (μm)	Absorption Coefficient (cm^{-1})	Damage Threshold (MW/cm^2)
$ZnGeP_2$	68.9	162	0.74-12	0.83	60
$AgGaSe_2$	32.6	63.3	0.71-18	0.089	2
$AgGaS_2$	12.5	12.8	0.47-13	0.04	25
$GaSe$	54	217	0.65-18	0.081	35
Tl_3AsSe_3	36.5	42.4	1.28-17	0.082	16
$CdGeAs_2$	217	1090	2.4-18	0.5	40

Table 1.1: Nonlinear optical crystals for mid-IR applications

ranges of 2.7-38.4 and 58.2-3540 μm, with typical linewidths of 6000 MHz, has been achieved for the first time.

1.2   Motivation

The doping with rare earth (RE) element in semiconductors has attracted considerable attentions. The fact is that RE element has partially filled $4f$ shells, which is well screened by outer closed orbitals of $5s^2$ and $5p^6$. The intracenter transitions of $4f$ electrons give rise to sharp, atom-like and temperature independent emission spectra in different host materials. Recently, the erbium ion, when incorporated into a semiconductor such as Si[20] or GaN[21], shows an intra-$4f$ transition at a wavelength of 1.54 μm, which is important as a light source in optical communication technology. Up to the present, only two research groups have studied the erbium-doped GaSe crystal (Er:GaSe). Lee et al.[22] used the optical absorption measurement to determine a direct energy gap of 1.79 eV and an indirect energy gap of 1.62 eV in Er:GaSe crystal at room temperature. Besides, an impurity optical absorption peak was found at

6

$6505 \ cm^{-1}$ (corresponding to the wavelength of 1.54 μm), which originated from the energy levels of erbium ions. Tagiev et al.[23] observed the luminescence excitation spectra of Er:GaSe crystal. But both of these groups did not discuss the photoluminescence property and electrical behaviors of Er-impurity in detail. In this thesis, we concentrate ourselves on the detailed results of photoluminescence property, Hall effect, deep-level transient spectroscopy (DLTS), and Er-related luminescence measurements in Er:GaSe crystal. The activation energies of acceptor impurity levels are deduced from the temperature dependent hole concentrations, DLTS, and Er-related luminescence measurements. Moreover, the radiative recombination mechanism and the role played by Er as a doping agent in GaSe is discussed. We also analyze the scattering dependent hole mobility in Er:GaSe at different temperatures.

Besides discussion on the optical and electrical properties of erbium doped GaSe in this thesis, using the undoped and erbium doped GaSe crystals to generate the mid-infrared coherent light source based on different-frequency generation are investigated. In the MIR fingerprint region from 2 to 20 μm, nearly all molecules exhibit strong fundamental rotational absorption lines and performance of spectroscopy is advantageous in this spectra region, securing sensitivity and selectivity. Available laser source in the MIR region, such as OPOs, color center lasers, and lead salt diode lasers which are the most popular laser sources for wavelength beyond 4 μm, are still limited due to small tuning range and low operating temperature requirements. CO_2 lasers which are commonly used in the 9-11 μm range, are also limited by narrow tunability and more important by the accidental coincidence between laser lines and absorption species of interest. Most recently, quantum cascade (QC) lasers, which cover wavelengths from 3.5 to 24 μm, can be operated either in cw mode at cryogenic

temperature or in pulsed mode at room temperature. However, in spite of their excellent spectroscopy properties in terms of power and linewidth, their tuning range is also limited and their beam divergence is poor. Therefore, difference frequency generation is still an important technique for the generation of narrow bandwith mid-infrared laser radiation with wide tunability. In this thesis, there are two parts of DFG system were used to generate nanosecond and picosecond mid-IR coherent light source. First, the difference frequency mixing of the Nd:YAG pumped periodical poled LiNbO$_3$ OPO output waves in GaSe crystal produced tunable nanosecond mid-IR from 4.35 to 14.25 μm. The other system, which consist of 1.064 μm pump and signal pulses of a parametric device based on a 10 Hz Nd:YAG amplifier, generated the picosecond mid-IR pulses in undoped and erbium doped GaSe crystals. The efficiency of the mixing and doping effect have been analyzed, considering these experimental results.

In order to satisfy the applications in nonlinear optics, the optical homogeneity, laser damage threshold, and crystal quality of GaSe are the main concerns. Due to conversion efficiency of DFG is proportional to the length of nonlinear crystal, scale-up the crystal size to achieve high efficiency and high-power output without sacrificing optical quality is also important. For these reasons, we make much effort on controlling the parameter of crystal growth to obtain the good crystal quality and centimeter size of GaSe.

1.3   Organization of This Dissertation

In this dissertation, we focus our efforts on the growth and characteristics of undoped and erbium doped GaSe crystals with different doping concentrations. In addition,

these crystals were also paid attention to investigate tunable mid-IR light source based on difference-frequency mixing. The outline is organized as follows: In chapter 2, we briefly describe the growth procedure of undoped and erbium doped GaSe crystals by Brigmam method. Furthermore, the structure and component of these asgrown GaSe crystals were analyzed by X-ray diffractometers and electron-probe X-ray microanalysis measurements, respectively. Besides, the optical characteristics were determined by photoluminescence and transmittance spectra in chapter 3. In contrast with undoped GaSe, new emission bands and absorption peaks were observed. Meanwhile, in order to explain the new emissions bands, the temperature and power dependence of photoluminescence technology were adopted to resolve this phenomenon. In chapter 4, impurities levels that resulted from doping erbium elements were studied by the temperature dependence of carrier concentration and DLTS measurements.

In chapter 5, the tunable and coherent nanosecond and picosecond radiation in mid-infrared by difference-frequency mixing in undoped and erbium doped GaSe crystals. The conversion efficiency and erbium doping effect were also discussed. In the final chapter, we make a briefly conclusion for this dissertation.

Chapter 2

Growth of GaSe Crystal

2.1 Introduction

GaSe compound has been the subject of several studies since the early 1970's, but it has some difficulties in growing good crystal quality with the techniques at that time. Afterward, there have been many attempts to grow GaSe crystals by Bridgman method and by vapor transport method. Vapor transport approach to grow GaSe crystal was extensively used between 1970 and 1987 by Cardetta et al.,[24] and Ishi et al.[25]. These researchers used (a) iodine transport, (b) close tube sublimation, (c) sublimation under the excess pressure of one of the parent components and (d) open tube sublimation. These authors had very limited success because they had no control on the kinetics and morphology. The iodine assisted transport and close tube sublimation produced flakes and plate type morphology. The transport under the excess Se pressures made a mixture of needles, rods, and occasionally plates. The open tube transport in the present of argon gas also produced ribbons and needles under large thermal gradient. These crystals were used to study various properties such as resistivity and mobility, photoconductivity and contact characteristics. Castellano and

Manfredotti [26] have shown that GaSe crystals can be used as the room temperature X-ray and gamma-ray detector material with reasonably unavailability of single GaSe crystals. In the melting growth method, the early attempts by Guseinov and Rasulov [27] produced mm size crystals, which were used to measure thermal conductivity. They used a growth speed of 14.5 to 29 cm/day, however, no data mentioned on thermal gradient and its effect on the quality of crystals. Additionally, Cardetta et al.[24] found that the crystal perfection depends on the lowering rate and on the ampoule diameter and that the crystal orientation depends on the bottom shape and on the position of the ampoule with respect to the furnace isotherms. Recently, Singh [28] used a numerical method involving the finite volume technique to optimize the furnace configuration. Besides, crystals were grown using the liquid encapsulated Bridgman (LEB) method in a vertical geometry during the growth procedure. The transparent nonreactive molten fluid, such as B_2O_3, were used to suppress the volatilization of selenium near the melting point. Therefore, good quality and centimeter size GaSe crystals with a diameter of 15 mm and a length of 8-12 mm could be fabricated. In addition to LEB method, we used a non-stoichiometric mixture of gallium and selenium with the 51.22 at.% of Se to overcome volatilization of selenium. The quartz tube with a capillary, which could suppress initially improper nucleation, was used in our procedure of growth. Accordingly, we are also able to obtain the centimeter size GaSe crystals with good crystal quality.

11

2.2　Experimental Procedure

2.2.1　Row Materials Preparation

As-supplied Ga was listed as 99.9999 % pure and Se listed as 99.999 % pure were employed. The GaSe mixture were prepared by mixing high purity Ga and Se in the non-stoichiometric ratio due to the volatile property of Se. According to the experience of our laboratory, 48.78 at.% of Ga and 51.22 at.% of Se were optimal non-stoichiometric ratio to overcome the volatilization of selenium. The mixture was placed in a well-cleaned quartz tube, which was cleaned by etching them in isopropyl alcohol, treated in hydrochloric acid, rinsed about five times with DI water, baked in a furnace at 600 ^{0}C in the atmosphere ambient for about 5 hours, and then cooled to room temperature. Subsequently, the quartz tube with GaSe mixture was sealed off at 10^{-6} Torr. The tube containing Ga and Se is then introduced into a vertical furnace that could rotate from clockwise 90^0 to anticlockwise 45^0 and the temperature carefully increased in steps till about 1050^0C. The slow increments in temperature are done to avoid an explosive reaction due to the high vapor pressure of Se. The sequence of each run is as following: room temperature to 1050^0C in 12 hours, held at 1050^0C and start to rotate the furnace for 12 hours, 1050^0C to room temperature in about 12 hours. This sequence has been successfully used to react Ga and Se to form a GaSe reaction mixture. The X-ray powder pattern will confirm the the formation of GaSe.

2.2.2　Crystal Growth

GaSe crystals were grown by a vertical Bridgman three-zone furnace, which was custom designed to achieve a temperature of 1100 ^{0}C and a gradient of 20 to 30

^{0}C/cm. Raw materials were enclosed in a well-cleaned quartz tube with a capillary under 10^{-6} Torr. The capillary helps to initiate the growth of single crystal of GaSe, and also helps in reducing the propagation of any defects such as dislocations and grain boundaries that might have started due to improper nucleation. The quartz tube is introduced into the furnace and the temperature of three zones raised to 1050 ^{0}C, 1050 ^{0}C and 600 ^{0}C, respectively. The temperature profile is shown in Figure 2.1 and the intention was to have a linear temperature gradient of about 25.5 ^{0}C/cm in the solidification regime of the crystal. The temperature stability of growth furnace with the standard deviation around 0.5 ^{0}C was monitored by R-type thermal couple. The stable temperature during growth can result in reducing the possibility of formation of nucleus. The melt of GaSe mixture homogenized and stabilized at about 970 ^{0}C for about 24 hours, after which the stepped motor is started which allows the tube to travel at a speed about 1.5-3 cm/day. Due to nonstability of the quartz tube during growth the main ingot containing the mixture can result in more than one crystal or poly-crystalline form. In order to reduce the perturbation from the stepped motor, each step moved only in 2.5 μm. As-grown crystals were cooled at the rate of 20 ^{0}C/hr. Once the process of growth is complete, the bottom of the ingot are removed and the GaSe crystals with the diameter of 10 mm and nearly 10 mm in length are obtained. Figure 2.2 shows an typical as-grown GaSe crystal.

Samples with faces perpendicular to the c axis were prepared from the ingot by cleaving and cutting with a razor blade and their typical dimensions were 4×4×0.3 mm^3.
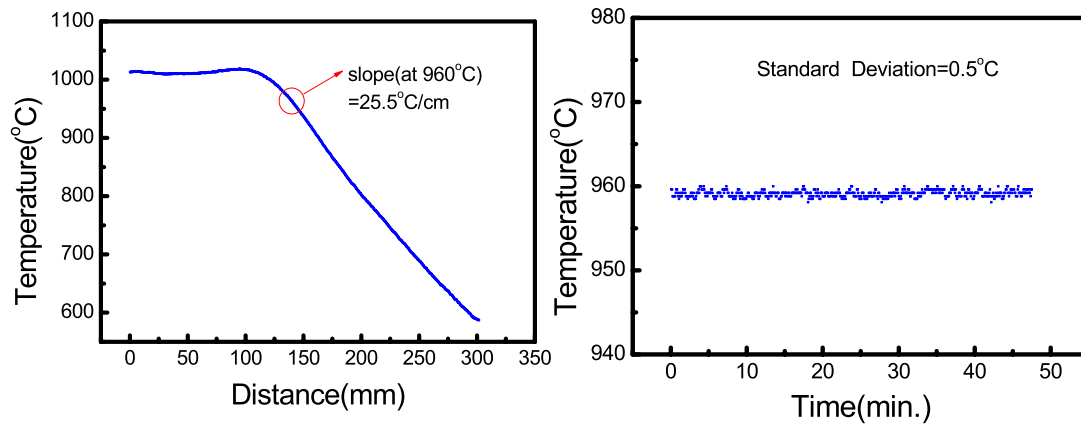
Figure 2.1: The temperature profile of Bridgman three-zone furnace (a) linear temperature gradient of about 25.5 ^{0}C/cm; (b) temperature stability.
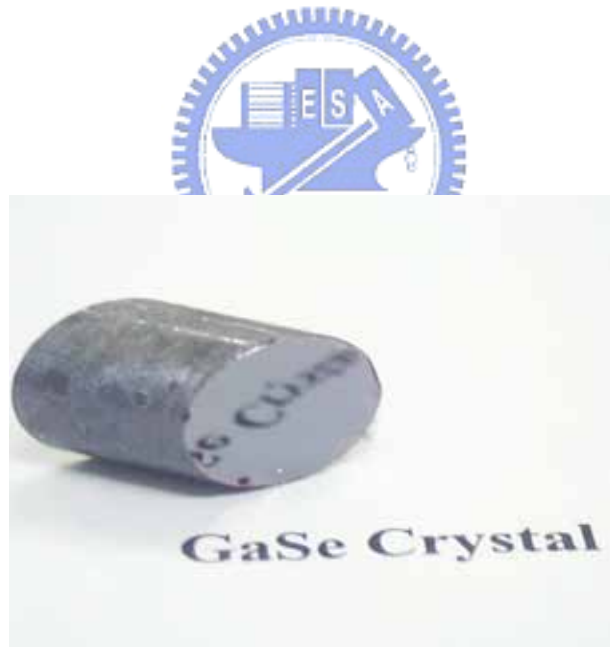
Figure 2.2: A cleaved surface of the as-grown crystal

14

2.2.3 Erbium-doped GaSe

GaSe was doped with pure erbium to investigate the optical and electrical properties. Er of 99.95 % purity was added to the reacted stoichiometic mixture of GaSe in the growth tube, evacuated, and sealed under 10^{-6} Torr. Different doping concentration of 0.2, 0.5 to 1 % at. and growth rates varying from 2-3 cm/day have been tested. In order to obtain more optically active erbium ions, the annealing process was used. Annealing of samples was carried out at 600 ^{0}C for 72 hours under excess Se atmosphere. Annealing showed significant improvement in erbium doped crystal.

2.3 Analysis of Structural Characteristics

The crystal structures of as-grown GaSe and Er:GaSe samples were observed using the X-ray diffractometers. Figure 2.3 displays the powder X-ray diffraction pattern of as-grown and annealed 1% Er:GaSe samples. Both samples present a clear appearance of a hexagonal structure of the <001> plane and these results are virtually the same as those for a pure GaSe sample. The estimated lattice constants are $a = 0.3751$ nm and $c = 1.588$ nm. By comparing the JCPDS value of ε-GaSe with $a = 0.3749$ nm and c = 1.5907 nm, the lattice constants of Er-doped samples are found in good agreement with those of GaSe although the radius of erbium atom is larger than that of gallium and selenium. Additionally, the thermal process under excess Se atmosphere at 600 ^{0}C for 72 hours does not change the hexagonal structure of Er:GaSe. When the doping erbium concentration is higher than 1 % at., the structure of crystal was obviously destroyed and the layered characteristic of crystal disappeared.

X-ray rocking curves of undoped and as-grown 1% Er:GaSe samples are shown in Fig. 2.4. In order to compare with the result of other groups, the plane of [008]
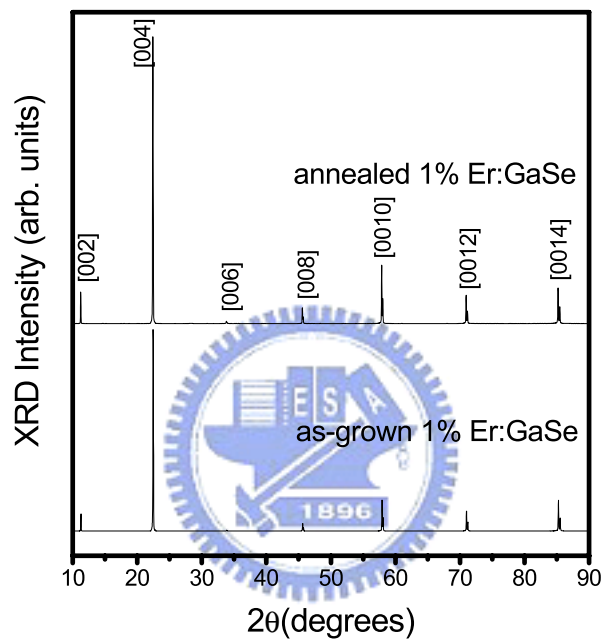
Figure 2.3: XRD patterns of as-grown and annealed 1% Er:GaSe samples
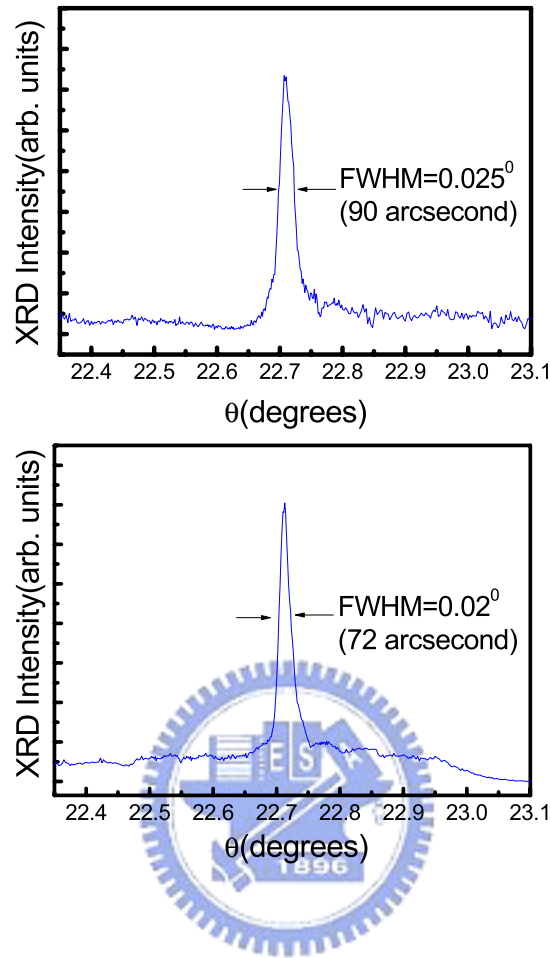
Figure 2.4: X-ray rocking curve of GaSe

was chose and measured. According to these results, there was no any sign of peak splitting, which indicate the absence of large angle grains. The full width at half maxima (FWHM) of [008] diffraction peak were 0.02^0 and 0.025^0 for undoped and 1% Er doped GaSe samples, respectively. These values of FWHM are much narrower than 0.15^o that was reported by *Singh*'s group [28]. Therefore, the undoped and Er doped GaSe crystals, which were grown by our laboratory, possessed the good crystal quality.

	Ga(%)	Se(%)	Er(%)
undoped GaSe	50.4408	49.5592	none
as-grown 1% Er:GaSe	50.9592	49.0038	0.0370
annealed 1% Er:GaSe	50.9882	48.9629	0.0489

Table 2.1: EPMA measurements

2.4　Analysis of Component Characteristics

The composition of all samples was measured by electron-probe X-ray microanalysis (EPMA). Table 2.1 lists the composition of GaSe and 1% Er:GaSe samples from EPMA measurements. These results reveal that the pure and Er-doped samples almost possess a Ga to Se ratio of 1:1. Besides, EPMA measurement can qualitatively confirm that erbium atoms were successfully doped in GaSe crystal. However, the initial Er concentration (Er~1%) added into the growth solution is about 10^{20} cm^{-3}. Our observed values of Er from EPMA listed in Table 2.1, are about three orders of magnitude lower than the initial Er concentration. It is not clear whether the remaining amounts of Er atoms are incorporated into the crystal or segregated during crystal growth. After the annealing process, an increase of ~30% Er concentration was observed in annealed samples.

18

2.5 Conclusions

The undoped and erbium doped GaSe crystals were successfully grown by the furnace of three temperature-zones with temperature gradient of 25.5^0C and temperature stability of 0.5^0C. The GaSe single crystals with a diameter of 10 mm and nearly 10 mm in length were obtained by non-stoichiometric mixture and quartz tube with a capillary. The ε-type GaSe with very good crystal quality were confirmed by X-ray diffractometer. EPMA measurement verified the composition of GaSe crystals in the stoichimetric ratio. Moreover, the erbium concentration of 10^{17} cm^{-3}, which were three order magnitude lower than the initial erbium concentration, were also detected. The result was not clear that the remaining amounts of erbium were incorporated into the crystal or segregated during crystal growth.

Chapter 3

Optical Properties of GaSe Doped with Erbium

3.1   Introduction

Photoluminescence is a common technique for identifying the energy-transfer processes and impurities levels of semiconductor compounds. It provides a non-destructive and non-contact method for examining the luminescent characteristics of materials. Actually, the photoluminescence of GaSe is quite complex at low temperature because of the particular GaSe band structure near the optical-absorption edge: the conduction band has an indirect minima at point M of the Brillouin zone, which is only 25 meV lower than the direct minimum (at Γ) and band structure of GaSe is shown in Fig. 3.1(a).[29] Optical transitions between these two minima of conduction band and the top of the valence band are full allowed, if the electric field of light is parallel to the c axis; for $\vec{E} \perp C$ the transition is weakly allowed, due to spin-orbit coupling, and its probability is about two orders of magnitude weaker than that for $\vec{E} \parallel$ c.[3] Therefore, these two minima can both be populated by the photoexcited carriers, and then
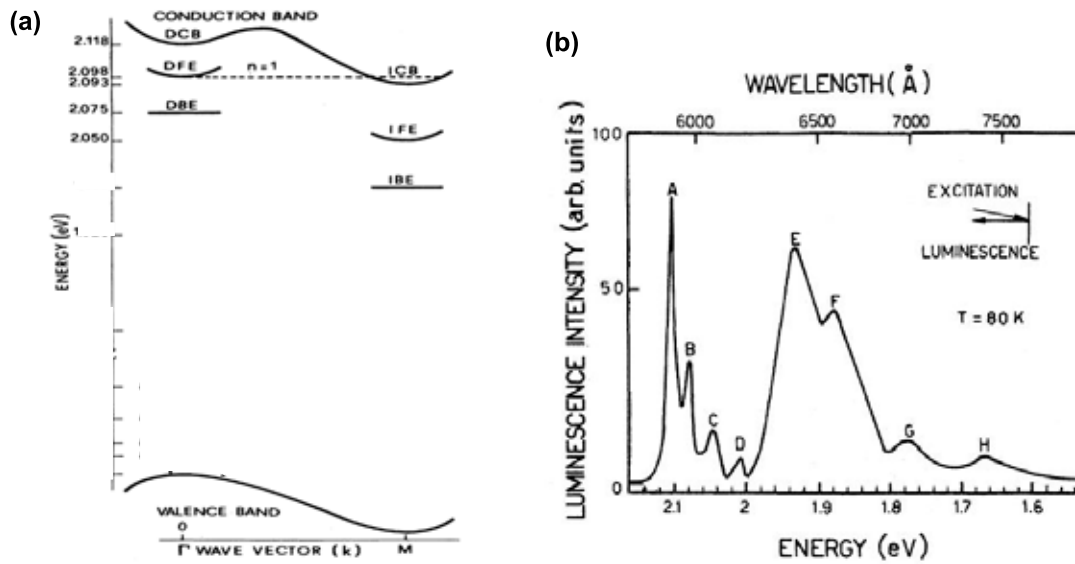
Figure 3.1: (a) Band structure of GaSe; (b) Typical photoluminescence spectrum of GaSe with intrinsic and extrinsic luminescence.

radiative recombination from states associated with direct and indirect gaps simultaneously occur. The shape of the photoluminescence spectra is therefore very sensitive to temperature, excitation intensity, and excitation energy.

Recently, the low-temperature photoluminescence of GaSe has been widely investigated by a number of authors, but there are considerable discrepancies between experimental findings of different research groups.[30, 29, 31, 32] This is in part due to the difficulties encountered in growing perfect single crystals and in part due to the not-well-known influence of impurities on the photoluminescence spectra. Capozzi *et al.*[30] have carried out luminescence at energy lower than absorption edge. They found that the extrinsic emissions are attributed to two competitive recombination

21

of donor-acceptor pair and free-electron-acceptor transitions under the different excitation intensity. Besides, the numbers of the additional exciton series with doublet character have been observed by Abdullaev *et al.*[33]. In general, the typical emission spectrum of GaSe single crystals is composed of two parts, within the range from 590 to 790 nm as shown in Fig. 3.1(b).[34] The high-energy part consists of relatively narrow lines (about 4 meV of half-width at 80K), ascribable to the free exciton and related recombination; the remaining part contains a group of broader lines (extrinsic luminescence) whose half-width range from 12 to 50 meV and which extends toward lower energies. The intensity of the exciton transitions is larger than extrinsic emission, which resulted from non-intentional doping of impurities.

The impurities levels of intentionally doped GaSe have been also extensively studied by use of the photoluminescence technique. In the Cu-doped GaSe samples, Capozzi *et al.*[3] found two new bands centered at 655 and 678 nm appear below the excitonic structure (80K). These bands are attributed to acceptor levels located at 0.031 and 0.093 eV above the valence band. The doping effect of nitrogen are also studied through photoluminescence measurement in the temperature ranges from 150 to 700 K and from 30 to 45 K, respectively by Chevy *et al.*[35]. Additionally, the doping elements of Ag, Mg, Zn, Cd, and P influence the photoluminescence spectra noticeably, which emitted different emission bands from the energy levels in the forbidden energy gap. The activation energies of the acceptor levels associated with the elements of Ag, Mg, Zn, Cd, and P have been reported by Shigetomi *et al.*[1, 2, 4, 36, 5]. Finally, defect centers in annealed p-GaSe crystals, which is associated with dislocations or stacking faults, have been investigated by using temperature dependence of photoluminescence intensity, peak energy, and FWHM.[37] In the recent years there

are also a lot of efforts on the doping with erbium element in semiconductor, which give rise to sharp, atom-like and temperature independent emission spectra. Due to those attractive characteristics, the optical properties of erbium doped GaSe were investigated by means of temperature and power dependent photoluminescence, and Fourier-transform infrared spectrometer measurements in this study.

3.2 Experiment and Measurement

By cleaving the GaSe ingots along the plane of layers, samples were obtained in the form of square platelets with area of 4×4 mm^2 and thickness of 0.1 to 0.5 mm. The optical transmission spectra in the near infrared region were determined by a Fourier-transform infrared spectrometer (FTIR, Bomem DA8.3) at room temperature.

For temperature dependence of photoluminescence measurement, samples were attached to the copper cold finger contained in a helium-cooled cryogenic system, which allows the variation of temperature between 7 and 300 K to be reached. In order to maintain the sample of a given temperature within $\pm$ 1 K in this range, the copper cold finger was equipped with a heater whose input can be controlled automatically. The surface of the samples were irradiated along c axis by a cw He-Cd laser with a wavelength of 325 nm. The emission was collected in the front scattering geometry from the face of crystal and analyzed by a TRAX320 monochromator. The luminescence was detected by a cooled photo-multiplier (PMT) and recorded by a personal computer. A set of neutral-density filter was used to changed the intensity of laser beam from 0.5 Wcm^{-2} to 50 Wcm^{-2}.

Measurement of photoluminescence in the near IR , Er-doped samples were excited using a 488 nm line output from an argon laser at an intensity of approximately 10 Wcm^{-2}. Luminescence was collected and dispersed with an HR1000 Jobin-Yvon monochromator. An InGaAs detector was used under cooling condition to measure the IR photoluminescence spectra.

3.3 Results and Discussion

3.3.1 Fourier-transform Infrared Spectroscopy
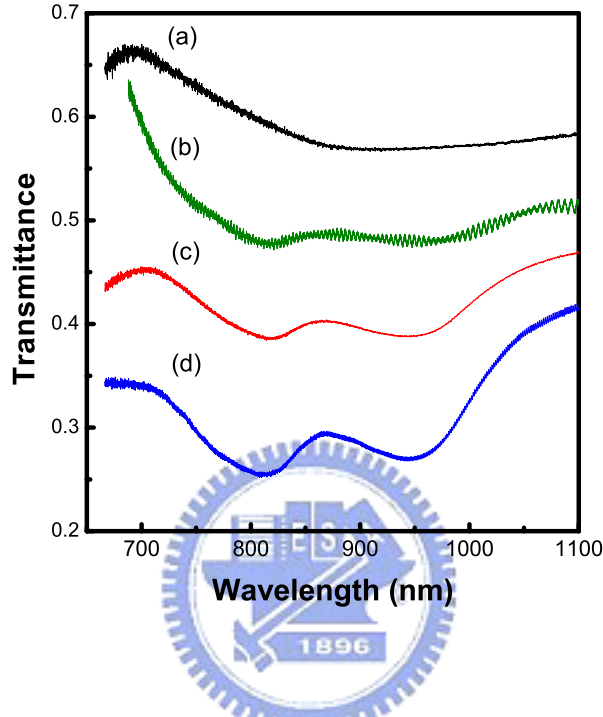
Figure 3.2: FTIR spectra of (a) undoped GaSe; (b)as-grown 0.5% Er:GaSe; (c) 1.0% Er:GaSe; and (d) annealed 1.0% Er:GaSe samples

Figure 3.2 shows FTIR transmission spectra of undoped GaSe, 0.5%, 1.0% Er:GaSe, and annealed 1.0% Er:GaSe samples at 300 K. The transmittance of undoped sample is always higher than those of Er-doped samples. It means that the erbium ions in GaSe crystal resemble the scattering centers to reduce the transmittance. The spectrum of undoped GaSe possessed smooth curve without any absorption peak throughout the range of measurement. In the near-IR region, two transmission valleys (absorption peaks) that appeared at ∼810 nm and ∼990 nm are observed in

0.5%, 1.0% Er:GaSe, and annealed 1.0% Er:GaSe samples. Observably, the transmission valleys in Er-doped samples showed strong increase for the added erbium concentrations. After annealed process, the transmission valleys were also enhanced. This phenomenon is probably due to the f-f transitions from $4f^n$ electrons, which are scarcely affected by the crystal fields around the erbium ions. Two transmission valleys are therefore assigned by the transition, $^4I_{9/2} \longrightarrow \, ^4I_{15/2}$ and $^4I_{11/2} \longrightarrow \, ^4I_{15/2}$ respectively. Based on the increasing the depths of the transmission valleys, we consider that the annealing process and increasing concentrations can enhance the erbium ions to be more active inside the crystal. However, we do not observe the transmission valley by the transition $^4I_{13/2} \longrightarrow \, ^4I_{15/2}$ of erbium ions at room temperature.

3.3.2 Temperature and Power Dependence of Photoluminescence
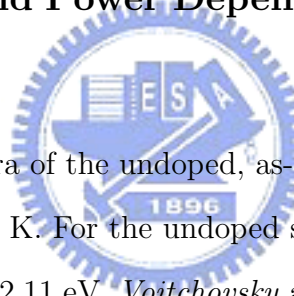
Figure 3.3 shows the PL spectra of the undoped, as-grown 0.2%, 0.5%, 1% Er:GaSe, and annealed 1% Er:GaSe at 7 K. For the undoped sample, only one emission band, denoted by A, was observed at 2.11 eV. *Voitchovsky* and *Mecier* [29] have shown that the emission peak due to the $n = 1$ exciton in GaSe at 77 K are detected at around 2.10 eV by using double spectrometer. The different peaks ascribed to the $n = 1$ exciton are components of fine structure which are induced by the different stacking configurations of γ and ε GaSe. Since the peak energy of 2.11 eV for the emission band A is included in the energy of the $n = 1$ exciton emission series, we consider that the emission band A is attributed to the recombination of the direct free exciton. The narrow linewidth of emission band A is estimated to be 2.29 meV, which indicated good quality crystal with low density of defects and cleaved without strains. In the
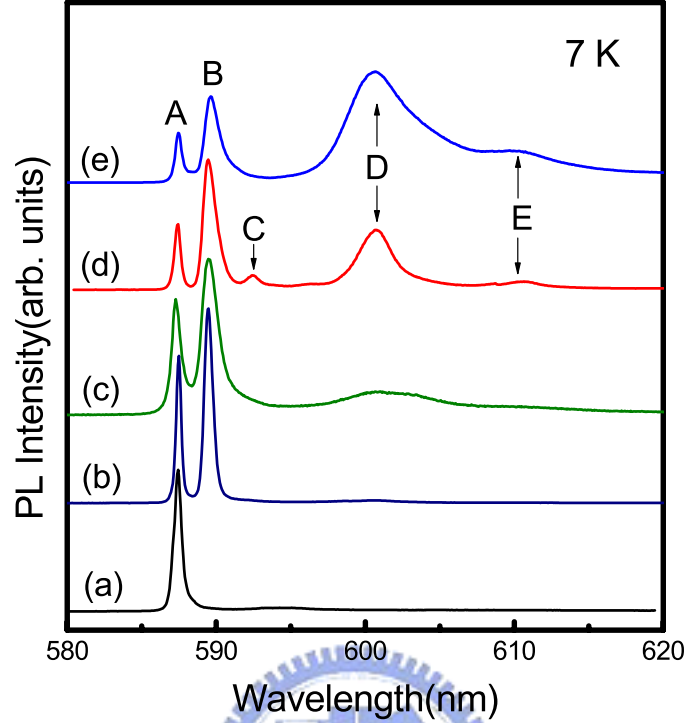
Figure 3.3: Photoluminescence spectra of (a) undoped GaSe; (b) 0.2% Er:GaSe; (c) 0.5% Er:GaSe; (d) 1.0% Er:GaSe; and (e) annealed 1.0% Er:GaSe samples at 7 K

as-grown 0.2%, 0.5%, 1% Er:GaSe, and annealed 1% Er-doped samples, the four new bands, denoted by B, C, D, and E, appeared at 2.103, 2.093, 2.064, and 2.032 eV, respectively. The PL intensity of emission bands B and D increased rapidly with increasing erbium concentration and is significantly influenced by adding erbium. For the as-grown and annealed 1% Er:GaSe samples, the emission bands C and E appears in addition to the emission bands B and D. Besides, the annealing process enhanced the PL intensity of the emission bands D and E, however, decreased the intensity of emission bands B and C. These four emission bands were formed on the lower energy
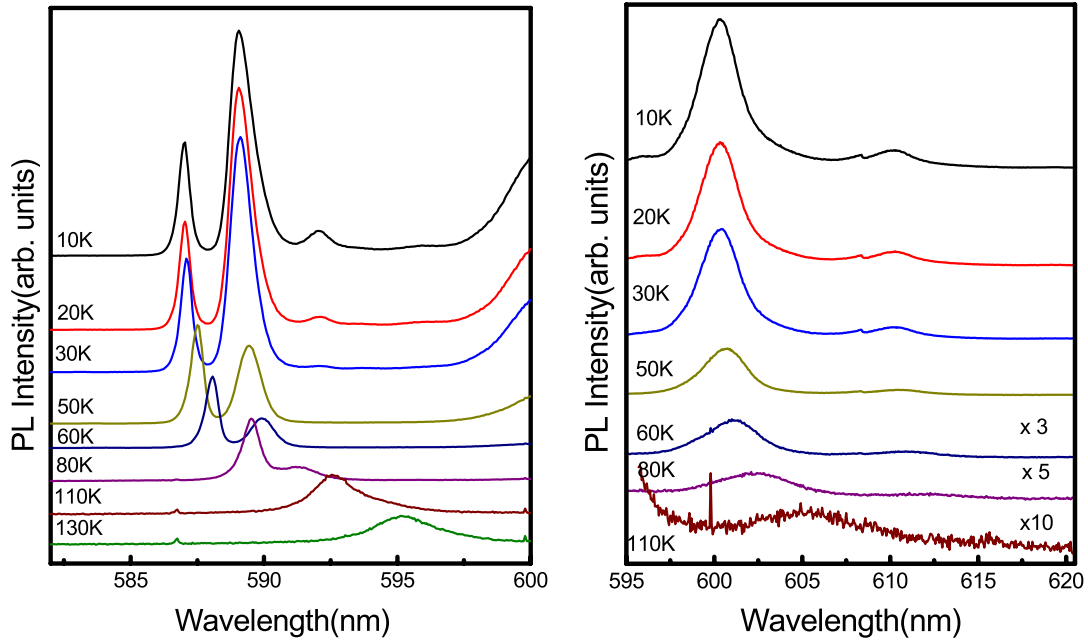
Figure 3.4: PL spectra of as-grown 1% Er-GaSe sample in the temperature range of 10-130 K.

side of free exciton and localized in the forbidden energy gap. We consider that the emission bands B, C, D, and E are contributed by doping impurities of erbium in GaSe. Because the temperature dependence of the observed photoluminescence spectra can give the information of the recombination mechanism. The radiative processes of these four emission bands were investigated by using the temperature dependence of the peak position of luminescence wavelength and the intensity.

Figure 3.4 shows the PL spectra of as-grown 1% Er-GaSe sample as measured in the 585-620 nm wavelength region and in the 10-130 K temperature range. The excitation laser intensity was constant at 10 Wcm^{-2}. The luminescence intensities of

five emission bands at different temperatures will be systematically analyzed and discussed. The temperature dependence data of luminescence intensities from emission bands A, B, and C in the as-grown 1% Er:GaSe sample are shown in Fig. 3.5. The intensities from B and C disappear rapidly between 40 K and 80 K as the temperature increases, however, the emission photoluminescence from A is further increased in this range. This behavior results from the change with temperature of the Fermi distribution of the electrons in the indirect band and the thermalization of electrons from the states related to emission bands B and C into the conduction band minima. However, similar decay behavior of luminescence intensities as a function of temperature has also been observed in Ref. [32]. According to Ref. [32], this phenomenon of the emission bands B and C is ascribed to photoluminescence from structural defects. Observably, the number of defects also increases with impurity content and decreases after annealing process.

The temperature dependence of peak energy from emission bands D and E are shown in Fig. 3.6. For comparison, the variation of the direct band-gap energy of GaSe as a function of temperature is also shown in this figure. Here, we evaluated the band-gap energy from the $n = 1$ exciton (peak A) by adding 19.5 meV, which is the value for the excitonic ionization energy (Rydberg energy) of the ground state. In Fig. 3.6, the variation of peak energy from D almost followed that of the band-gap energy of GaSe. Main luminescence mechanisms related with the impurity levels in semiconductor are considered to be the impurity-band or donor-acceptor transitions. The peak energy due to the impurity-band transition decreases with the band-gap energy as temperature increases. Similar temperature dependent behavior of peak energy has been observed in the donor-acceptor transition. The negative-temperature
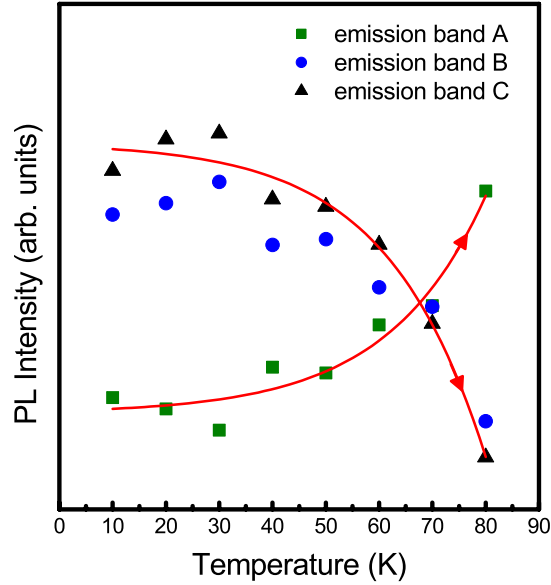
Figure 3.5: Comparison of temperature dependent PL intensities from emission bands A, B, and C

shift of the donor-acceptor emission was explained by the transition involving acceptor and relatively deep donor levels. These results indicate that the emission band D might be attributed to the transition from the conduction band to the impurity level or from the impurity level to the valence band. In an attempt to determine whether the mechanism of the emission band D, we measured the temperature dependence of luminescence intensity of the emission band D.

The behavior from thermal quenching of the emission band D in the samples doped with Er of 0.5% and 1% is shown in Fig. 3.7. The luminescence intensity gradually decreased with increasing temperatures between 10 and 50 K. At temperature above 50 K, semilog plots of luminescence intensity as a function of reciprocal temperature gave an almost straight line. The variation of luminescence intensity
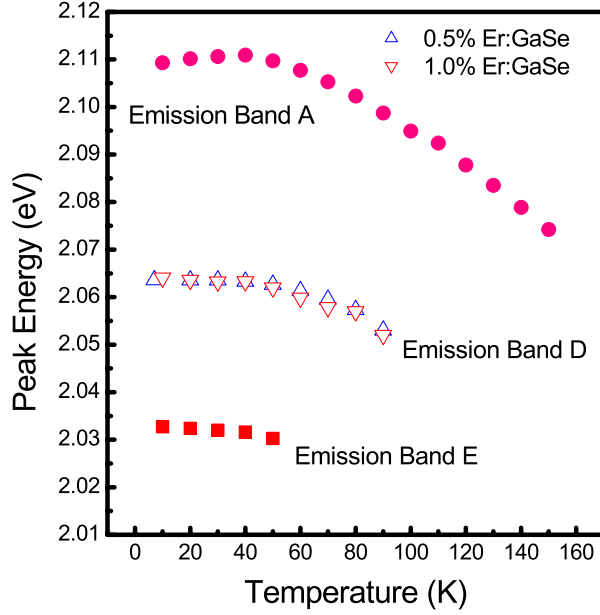
Figure 3.6: Temperature dependence of the peak energy of emission bands A, D, and E

I(T) with temperature T can be described by

$$I(T) = \frac{I_0}{1 + c\exp(-\frac{E_a}{kT})} \tag{3.1}$$

where I_0 is the luminescence intensity as T approaches 0 K, c is a temperature-independent constant, k is Boltzmann's constant and E_a is activation energy. The solid lines in Fig. 3.8 fit both the 0.5% and 1% samples. The activation energies of about 64.2 meV and 61.4 meV are obtained from the 0.5% and 1% samples, respectively. Among the rare earth doped semiconductors, such as InP:Er, GaAs:Nd, and InP:Nd, the similar trap level ranging from 80-120 meV exists in those host-materials.[38] Besides, the sum of the 2.064 eV emission peak (Band D) energy and

31
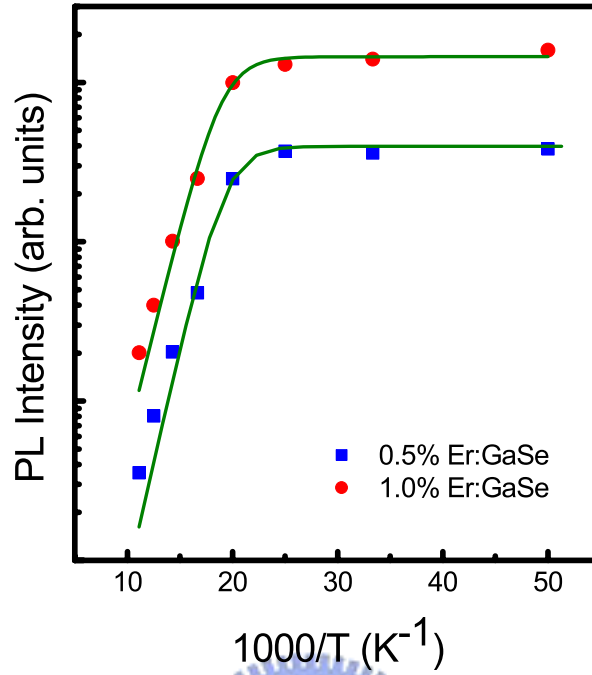
Figure 3.7: Variation of PL intensity with reciprocal temperature for the D emission band

the $\sim$64 meV thermal quenching activation energy from the emission band D agrees with the band-gap energy of GaSe. According to the electrical results of Hall measurement, the radiative transition from D can be explained by the impurity-band recombination and the impurity level is at $\sim$64meV above the valence band. In Fig. 3.3, PL intensity from emission band D at 2.064 eV increases through the annealing process. This result is consistent with those of FTIR transmission spectra. Additionally, the temperature dependence of peak energy from E is also revealed in Fig. 3.6. The intensities of emission band E disappear rapidly at 50 K as temperature

32

increases. Therefore, the PL peak from E at 2.032 eV might be due to the one-LO-phonon replica of the band-impurity recombination at 2.064 eV, because the energy difference between D and E matches that of the E_2' (LO) mode which is 31.25 meV ($252\ cm^{-1}$).
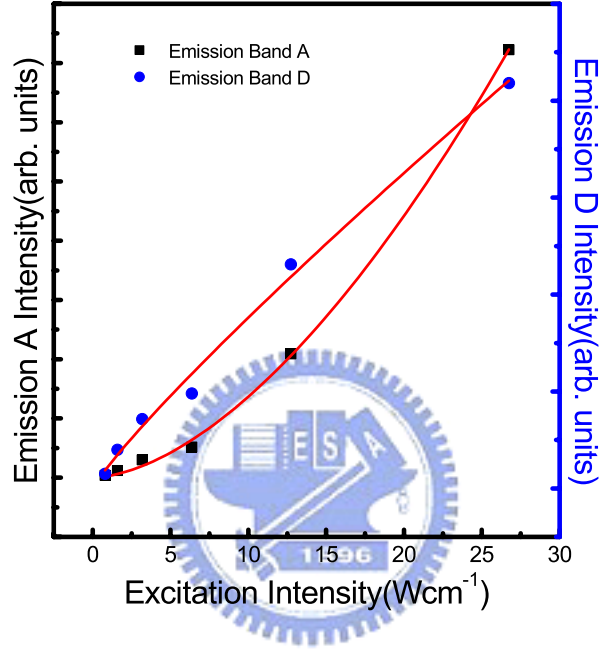
Figure 3.8: Dependencies of the luminescence intensity at emission bands A and D maximum versus excitation laser intensity at T = 7 K. The solid curves give the theoretical fits using Eg. (2).

In order to study the luminescence mechanism of emission band D, the laser excitation intensity dependence of the observed photoluminescence spectra was used to provide valuable information about the recombination mechanism responsible for the observed luminescence. As in the case of temperature dependence, a deconvolution

procedure was applied to analyze the excitation power dependent behavior of luminescence spectra. From such analysis, we get the information about the intensities for the emission bands A and D at different laser excitation intensities. The plot in Fig. 3.8 shows the excitation laser intensity as a function of the luminescence intensity of emission bands A and D at 7 K. The experimental data in Fig. 3.8 can be fitted by the simple power law of form[31]

$$I \propto L^{\gamma} \tag{3.2}$$

where I corresponds to the luminescence intensity, L corresponds to excitation laser intensity and γ is a dimensionless constant. It was found that luminescence intensity at emission bands A and D increases sublinearly with increase of excitation intensity with the values of $\gamma = 1.693$ and 0.885, respectively. It is well known that for excitation laser photon energy exceeding the band gap energy E_g, the exponent γ is generally $1 < \gamma < 2$ for free and bound exciton emission, whereas $0 < \gamma \leq 1$ for free-to-bound and donor-acceptor pair recombination.[31] According to the fitting results, emission bands A and D could be attributed to recombination of direct free exciton and impurity-band recombination, respectively. This analysis of observed luminescence spectra as a function of excitation laser intensity is consistent with those of temperature dependent luminescence spectra.

3.3.3 Erbium Related Photoluminescence

As shown in Fig. 3.9(a), strong luminescence emissions from intra-$4f$ shell transitions associated with Er^{3+} are revealed in as-grown and annealed 1% Er:GaSe at low temperatures. The $4f$ levels are determined in terms of angular quantum number J
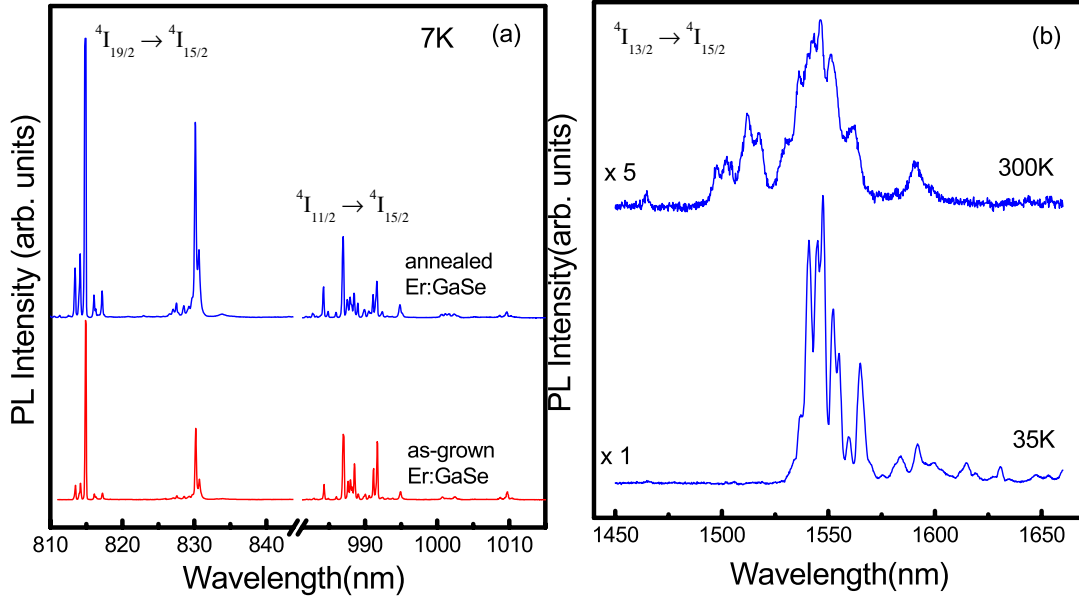
Figure 3.9: (a)Near-infrared PL spectra of $^4I_{9/2} \longrightarrow {}^4I_{15/2}$ and $^4I_{11/2} \longrightarrow {}^4I_{15/2}$ transitions of Er^{3+} in Er:GaSe samples at 7 K. (b)Er-related luminescence around 1.54 μm in 0.5% Er:GaSe at 35 K and room temperature.

and are split into several sublevels by the Stark effect in the crystal field. Therefore, it depicts the infrared spectra that exhibit a characteristic luminescence at 0.81 μm, 0.99 μm and 1.54 μm arising from the intracenter transitions $^4I_{9/2} \longrightarrow {}^4I_{15/2}$, $^4I_{11/2} \longrightarrow {}^4I_{15/2}$, and $^4I_{13/2} \longrightarrow {}^4I_{15/2}$ of erbium ions in Er:GaSe at low temperatures. Besides, the annealed Er:GaSe observably exhibits stronger infrared luminescence than the as-grown one. We believe that more erbium ions become active through the annealing process.

As well as measurements of the near-band-edge luminescence spectra of Er:GaSe,

measurements of Er-related luminescence due to carrier transitions yields more information about the level of impurities. The $4f$-shell luminescence is involved in transferring energy from the semiconductor host to the Er $4f$ core via Er-related defects, so luminescence associated with $4f$-shell transition can be observed. Figure
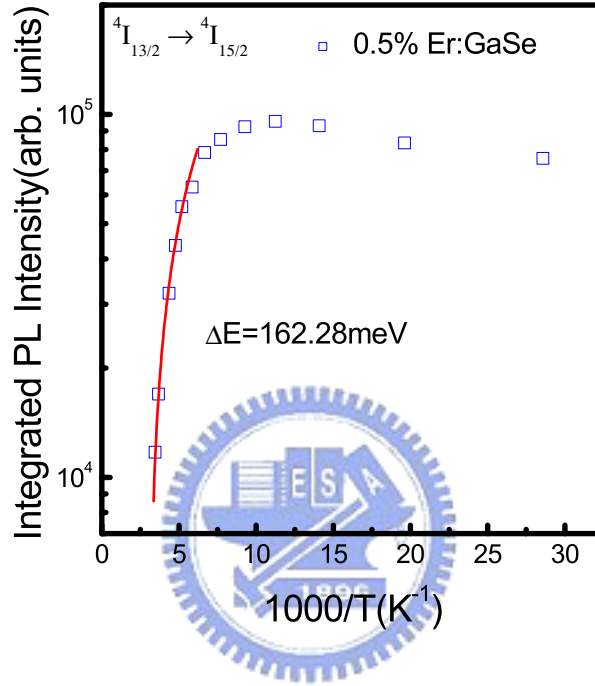
Figure 3.10: Temperature dependence of the integrated intensity for $^4\mathrm{I}_{13/2} \longrightarrow {}^4\mathrm{I}_{15/2}$ emission.

3.9(b) shows the PL spectra of Er-related intra-$4f$-shell luminescence from a 0.5% Er:GaSe sample at 35 K and at room temperature (300 K). The peak wavelength at around 1.54 μm is associated with a transition from two spin-orbit interacting related manifolds $\left({}^4\mathrm{I}_{13/2} \longrightarrow {}^4\mathrm{I}_{15/2}\right)$. Apart from the peak at a wavelength of 1.54 μm, various additional peaks appeared at shorter wavelengths ($\sim$1.52 μm) as the temperature increased to 300 K. The additional peaks correspond to the splitting

patterns of the ground manifold (^{4}I$_{15/2}$) due to the surrounding crystal-field caused by host atoms that surround Er. The main peaks ($\sim$1.54 μm) do not shift to longer wavelength over this wide range of temperatures because the intra-4f transitions are shielded by the outer closed orbits. However, the integrated intensity is quenched by a factor of approximately 5 as the temperature is increased to 300 K. Figure 3.9 displays the Arrhenius plot of the thermal quenching of the integrated intensity. At high temperature, the intensity is reduced with an activation energy of about 162 meV. This value is almost the same as that of the deep acceptor level revealed by DLTS measurements. Similar behavior has also been reported to be exhibited by Er-doped GaAs and Yb-doped InP,[39] whose excitation mechanisms have been comprehensively studied. Two different processes may be responsible for the decrease in the intensity. One is believed to involve the back-transfer of energy. This mechanism is simply the reverse of Er^{3+} excitation; the excited Er^{3+} ion decays by promoting holes from the conduction band to an Er-related deep acceptor level in the GaSe band gap, forming an electron-hole pair. The pair thermally dissociates at elevated temperature, resulting in the quenching of luminescence. Note that this process is exactly the reverse of excitation, hence the name back-transfer since the energy is transferred back through the same path. The other is that the number of electron-hole pairs at deep acceptor level decrease due to the thermal emission of carriers from level as temperature increases before its energy transferring to the Er 4f-shell.

3.4 Conclusions

Photoluminescence and FTIR measurements on Er:GaSe samples with different erbium concentration have been carried out. Temperature dependent photoluminescence measurement has shown that radiative transition with erbium atoms was primarily caused by an acceptor level at 2.064 eV. The emission band at 2.032 eV might be due to the one-LO-phonon replica of the band-impurity recombination at 2.064 eV. The emission bands at 2.103 eV and 2.093 eV are ascribed to structural defects based on the temperature dependence of PL intensities. Besides, the recombination of direct free exciton and impurity-band transition were also confirmed by power dependent photoluminescence measurement. The infrared luminescence and transmission spectra that arise from the intracenter transitions $^4I_{9/2} \longrightarrow {}^4I_{15/2}$, $^4I_{11/2} \longrightarrow {}^4I_{15/2}$, and $^4I_{13/2} \longrightarrow {}^4I_{15/2}$ of erbium ions are observed. Finally, the deep accepter level that located at 162 meV above the valence band was believed to involve the the thermal quenching of Er-related luminescence.

Chapter 4

Electrical Properties of GaSe Doped with Erbium

4.1 Introduction

GaSe is a layer semiconductor with the band gap of about 2.0 eV at room temperature. In view of its possible application in photoelectronic devices in the visible range, a great deal of attention has been devoted to the study of the GaSe doped with impurities. Because the applications of semiconductor are governed by electrical properties, which are strongly influenced by the presence in the forbidden gap of energy levels, arising from chemical impurities and/or structural defect. In this issue, detailed information on doping processes plays an important role. The problem of doping, which was investigated early, has been recently approached by other groups that have specially studied the influence of impurities from group I and II as acceptors in GaSe. In general, the temperature dependence of Hall effect measurement and deep level transient spectroscopy(DLTS) were used to the study of electrical properties in GaSe crystal with dopants. The temperature dependence carrier concentration and mobility could present location and concentration of impurity levels and electrical

39

transport behavior of doped GaSe crystal, respectively. In addition, DLTS measurement can examine the existence of deep traps in the band gap of GaSe crystal with different dopants. Therefore, the hole concentration and the mobility on the order of $10^{15} - 10^{16}$ cm^{-3} and $12 - 66$ cm^2/Vs, respectively, at room-temperature have been demonstrated by doping Cd, Zn, Cu, and Ag.[2, 4, 5, 40] Activation energies for hole concentration are on the order of 300 meV for Cd, Zn, and Mn doped GaSe, of 40 and 140 meV for Cu-doped samples, and of 60 meV for Ag-doped samples. Until now only the dopants of Sn, Cl and I could act as donors in GaSe samples.[6, 7, 8] The electron concentration for n-type GaSe are on the order of $10^{12} - 10^{13}$ cm^{-3} at room-temperature. Attempts to get lower resistivity in n-type GaSe have not been demonstrated.

The transport properties of GaSe along the layers have been widely investigated in the past years.[6, 7, 41] The factor is that GaSe crystallizes in a layer structure and each layer consists essentially of two layers of Ga atoms sandwiched between two layers of Se atoms. Inside the layers, the bonding is largely covalent, between them it is Van der waals. This highly dissymmetrical property between bond strengths in intra- and inter-layer gives rise to a strong scattering of the charge carriers by optical phonons polarized perpendicular to the layers. Besides, the transport properties of tin and nitrogen doped p-GaSe crystal have been analyzed in the framework of the Schmid and Fivaz model.[41] In the results of different tin concentration doped p-GaSe crystals, transport behavior is proposed to relate to impurity paring effects giving rise to thermal shallow acceptors with low ionization energy and low carrier scattering cross section which make the hole mobility to be controlled by phonon scattering mechanisms even for relatively high impurity content.[6] As for nitrogen doped p-GaSe

40

crystal, two phonon scattering mechanisms, which are the scattering by 16.7 meV $A_1^{'}$ homopolar optical phonon with a hole-phonon coupling constant $g^2=0.115$ and the scattering by 31.5 meV LO polar phonon with a hole Fröhlich constant $\alpha_{h\perp}=0.741$ were considered in order to quantitative account of the temperature dependence of the hole mobility.

In this article the temperature dependence of Hall effect and DLTS measurements were used to discuss about the electrical and transport properties of GaSe single crystals doped with different amounts of erbium in the temperature range from 77 to 300 K.

4.2 Experimental Methods and Principles

The Hall measurements were made using a four-point direct current Van der Pauw configuration at temperatures between 80 and 300 K, to obtain the temperature dependent effects on the concentration and mobility of carriers. The current was made to flow in c surface planes and a magnetic field ($\sim$0.5 T) was applied perpendicular to these planes simultaneously. The metal contacts were soldered using high-purity indium and then heated to 600 K for 10 minutes at 10^{-6} Torr to improve the ohmicity of the contact. The DLTS measurements were made on the Schottky barriers diode, which was formed by thermally evaporating Au onto a c surface plane. The pattern of the Schottky contact was a circle with a diameter of approximately 1mm. The ohmic contact was formed on the same side by soldering high-purity indium. The Au/p-GaSe Schottky diodes exhibited good rectification characteristics when it is forward-biased. Each diode had an effective barrier height of 0.68 eV and forward characteristics with an ideality factor of n = 1.79 at room temperature. This high ideality factor may be partially related to the defects, caused by the preparing of the surface of the semiconductor.

DLTS measurements were made at a bias of -1 V, pulsed periodically to 0 V to fill the traps. Transient capacitance signals were obtained using a test AC signal at 1 KHz with an amplitude of 100 mV at temperatures from 130 to 380 K. The error in the measured temperature was estimated to be under 1 K when the measurement was made.

4.3 Results and Discussion

4.3.1 Temperature Dependence of Hole Concentration

The hole concentration was determined from the Hall measurements, by assuming a unit Hall factor.[42] Table I lists the typical resistivity, hole mobility and hole concentration of three different Er:GaSe samples, at room temperature. The values are compared with those of the undoped GaSe, which was grown under the same conditions. The estimated hole concentration increased from $\sim 1.5 \times 10^{17}$ to $\sim 6 \times 10^{17} cm^{-3}$ in samples as the concentration of dopants increased from 0.2 to 1 at. %; these values are one order of magnitude higher than those obtained with other dopants, as reported in GaSe.[6]
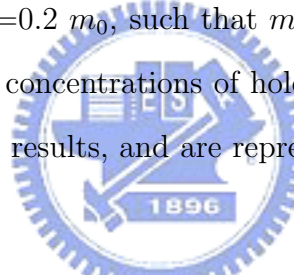
Initial Er concentration (at. %)	Hole Concentration (cm^{-3})	Mobility $(cm^2/V \cdot s)$	Resistivity $(\Omega - cm)$
undoped GaSe	1.058×10^{17}	56.76	104
0.2% GaSe:Er	1.529×10^{17}	34.073	1.199
0.5% GaSe:Er	2.084×10^{17}	23.358	1.283
1.0% GaSe:Er	4.132×10^{17}	22.44	0.784

Table 4.1: The results of Hall effect measurement.

Figure 4.1 plots the temperature-dependent hole concentration of three different Er:GaSe samples. Throughout the range of temperatures, the hole concentration in Er:GaSe samples increases with temperature. The temperature-dependence of the carrier concentration can be interpreted by assuming that the semiconductor contains two acceptor levels, with ionization energies of E_{a1} and E_{a2}, respectively. The following cubic equation for hole concentration can be easily obtained by applying the neutrality condition under the non-degenerate assumption.[43]

$$p = \frac{N_{a1}}{1 + \frac{\beta p}{N_v} \exp(\frac{E_{a1}}{k_B T})} + \frac{N_{a2}}{1 + \frac{\beta p}{N_v} \exp(\frac{E_{a2}}{k_B T})} \qquad (4.1)$$

where p represents the hole concentration; T is the absolute temperature; N_{a1} and N_{a2} are the doping concentrations of the acceptor impurities; k_B is the Boltzmann constant, and β is the degeneracy factor, which is taken to be 2 in this calculation. In Eq. (3), the density of states N_v and the effective mass m_v^* of the valence band are $N_v = 4.83 \times 10^{15} T^{3/2} (m_v^*/m_0)^{3/2}$ and $m_v^* = ((m_{h\perp}^*)^2 m_{h\parallel}^*)^{1/3}$, respectively, where m_0, $m_{h\perp}^*$ and $m_{h\parallel}^*$ are the free electron mass, the effective hole mass perpendicular to the (100) plane, and that parallel to the (100) plane respectively. Here, the effective hole masses $m_{h\perp}^* = 0.8$ m_0 and $m_{h\parallel}^* = 0.2$ m_0, such that $m_v^* = 0.5$ m_0, are used in Eq. 4.1. The best fitting curves for the concentrations of holes in three different samples are quite close to the experimental results, and are represented by the solid lines in Fig. 4.1.

Initial Er concentration (at. %)	N_{a1} (cm^{-3})	N_{a2} (cm^{-3})	E_{a1} (meV)	E_{a2} (meV)
0.2% GaSe:Er	3.116×10^{15}	5.549×10^{17}	67.76	156.94
0.5% GaSe:Er	1.791×10^{16}	1.291×10^{18}	67.13	158
1.0% GaSe:Er	8.504×10^{16}	4.506×10^{18}	63.26	160.75

Table 4.2: The parameters of fitting results from temperature dependence of Hall effect measurement.

Table II lists values of N_{a1}, N_{a2}, E_{a1}, and E_{a2} obtained from various samples. The deep and shallow acceptor energy levels are located at around 158 ± 3 and 65 ± 3 meV above the top of the valance band. The concentration increased with
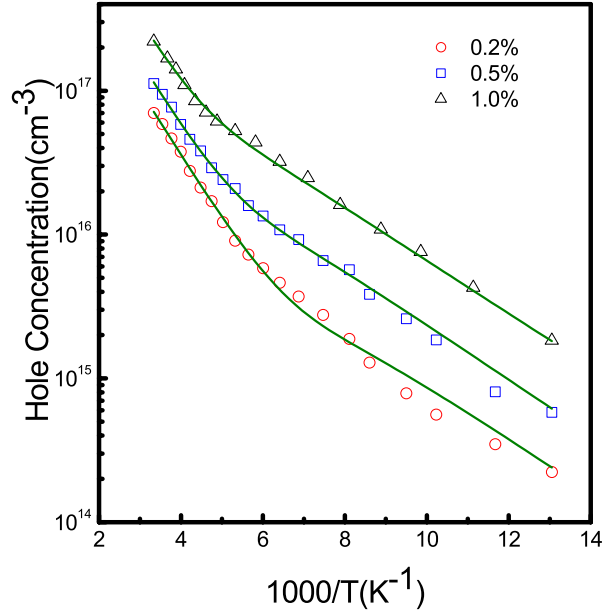
Figure 4.1: Hole concentrations as a function of reciprocal temperature in Er:GaSe samples. The solid lines show the calculated hole concentrations from Eq. 4.1.

increasing erbium concentration in all Er:GaSe samples, at all levels of impurities. A comparison of the impurity level at an ionization energy of 65 meV obtained from Hall measurements with that obtained by photoluminescence measurement,[44] revealed that this acceptor state was not only a radiative center, but also electrically active.

The doping of GaSe with erbium is now considered. Before the acceptor configuration can be explained with reference to the impurity Er in GaSe, the reader should be aware that similar rare earth elements, such as gadolinium (Gd), doped in GaSe have been examined by electron paramagnetic resonance (EPR) spectroscopy.[45] The doping process has been established to involve the replacement of one covalent-bound pair of gallium Ga_2^{4+} atoms with one Gd^{3+} atom, which acts as an acceptor. The

45

configuration of acceptors in GaSe has been speculated to be determined by the sub-stitution of one Er^{3+} atom for one pair of Ga^{2+} atoms. In another possible model, Er^{3+} ions are interstitial at interlayer sites, corresponding to sites in between two layers of Se atoms, and bond with Se atoms in the octahedral configuration. This configuration will yield a Ga vacancy, which contribute to the character of the accep-tor. Therefore, two acceptor levels are probably associated with Er atoms that are involved in the substitutional and interstitial processes in GaSe.

4.3.2 Temperature Dependence of Mobility

The temperature dependence of the hole mobility follows the trends of previously reported results. The hole mobility was determined by considering the mechanisms of scattering from both homopolar optical phonon and ionized impurities:

i) Scattering due to 16.7 meV A_1' homopolar optical phonon can be described using the Fivaz-Schmid relaxation time.[41]

$$\tau = \frac{\hbar(\hbar\omega)^{1/2}}{3\sqrt{\pi}g^2(k_BT)^{3/2}} \tag{4.2}$$

where g is a coupling constant for intraband interactions between three-dimensional carriers and $\hbar\omega$ the homopolar optical branch, and is the energy of the optical phonon.

ii) Scattering due to ionized impurities is accounted for in the relaxation time approximation according to the known Brooks-Herring formula;[46]

$$\tau_{ion} = \frac{2^{7/2}m^{1/2}(4\pi\varepsilon)^2(k_BT)^{3/2}}{\pi^{3/2}e^4Z^2N_i[\ln(1+\beta) - \frac{\beta}{1+\beta}]} \tag{4.3}$$

where $\beta = (24m\varepsilon/n)(k_B T/e\hbar)^2$; N_i and eZ represent the concentration of

ionized impurity, and the ionic charge of the impurity, respectively.
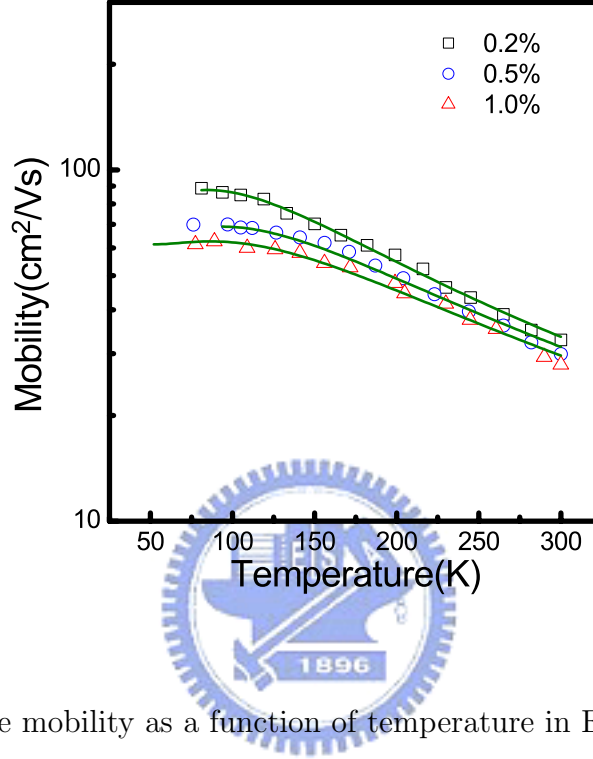
Figure 4.2: Hole mobility as a function of temperature in Er:GaSe samples.

Figure 4.2 plots the temperature-dependence of the hole mobility in GaSe crystals with different amounts of erbium. The hall mobility in Er:GaSe samples decreases as the temperature increases in the range 80-300 K. In order to analyze those results, it is introduced in the elastic term of the homopolar phonon and ionized impurity scattering rates in the iteration method. The solid lines in Fig. 4.2 represent the results of this calculation. The theoretical behavior is experimentally supported at various doping concentrations in Er:GaSe samples over the whole range of temperatures. The hole-phonon coupling constant (g^2) was determined to be 0.235, 0.243 and 0.252 at

0.2 %, 0.5 % and 1.0 % Er:GaSe, respectively. At low temperatures, the hall mobility is limited by ionized impurity scattering, while at higher temperatures, the mobility of hole carriers is probably limited by the short-range interaction with homopolar optical phonons, polarized normally to the layers. The mechanism by which neutral impurities are scattered has not yet been elucidated. The Erginsoy relaxation time[47] of neutral impurities indicates that the mobility of holes can be affected when it is in the order of 10^4 $cm^2/V \cdot s$ at 300 K, which greatly exceeds the values measured herein; therefore, the neutral scattering mechanism is negligible herein.

4.3.3 Thermal Annealing Effects of Au Schottky Contact on p-GaSe

In Fig. 4-3 we present the I-V characteristics of Au Schottky contact on 0.2 % Er:GaSe sample which is annealed for 10 min at various temperatures from 200 to 500 ^{0}C. As the annealing temperature is higher than 500 ^{0}C, the crack and damage on the surface could be observed easily by a naked eye. The factor is that higher temperature would evaporate the Se out of the surface from GaSe. Shigetomi et al.[37] verified the similar results by photoluminescence and X-ray diffraction measurements. A new emission band with 1.45 eV that is related to the Se vacancy-acceptor complex was observed in the PL spectra of the samples after annealing at 600 ^{0}C. For comparison, the result of as-deposited sample is also included in this figure. As can be seen in this figure, the reverse leakage current for the Schottky contact tends to decrease significantly by several order of magnitude as the annealing temperature is increased from 200 to 400 ^{0}C, it then increased further increase of annealing temperature up to a temperature of 500 ^{0}C. Clearer picture can be redraw the reverse leakage current density measured
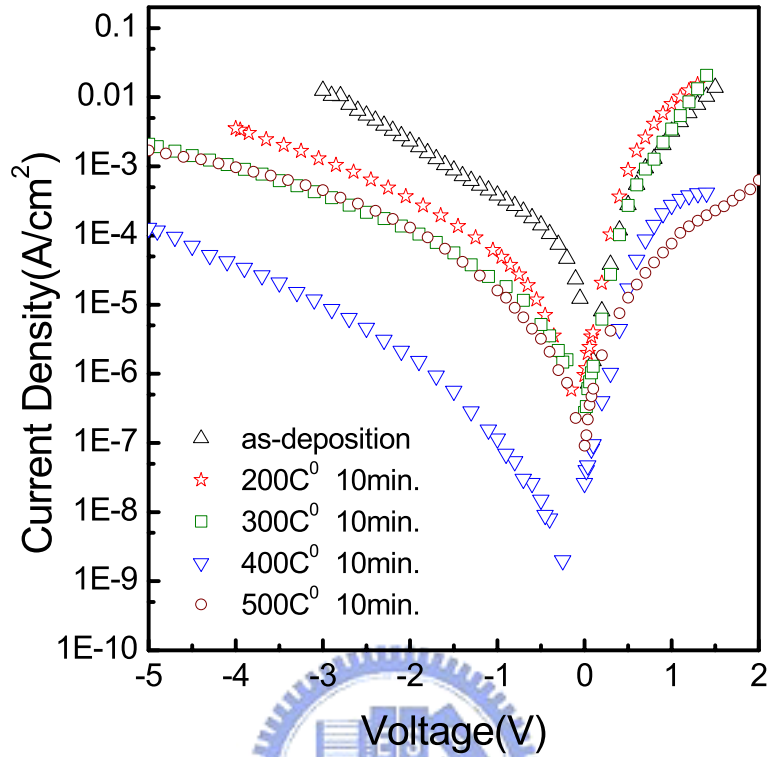
Figure 4.3: The I-V characteristics of Au Schottky contact on p-GaSe which were annealed for 10 min. at various temperature from 200 to 500 ^{0}C.

at -3 V against the annealing temperature in Fig. 4-4. Note that intolerable high leakage currents are resulted from the as-deposited and low temperature (≤ 400 ^{0}C) annealed samples. On the contrary, fairly good rectifying characteristics can be obtained around annealing temperature of 400 ^{0}C. The corresponding reverse leakage current is as low as 1.0×10^{-5} A/cm^2.

In addition to the leakage current, the forward current-voltage characteristics such as barrier height and ideality factor are known the primary factors concerning the performance of a Schottky contact. In thermionic-emission theory, the assumption is
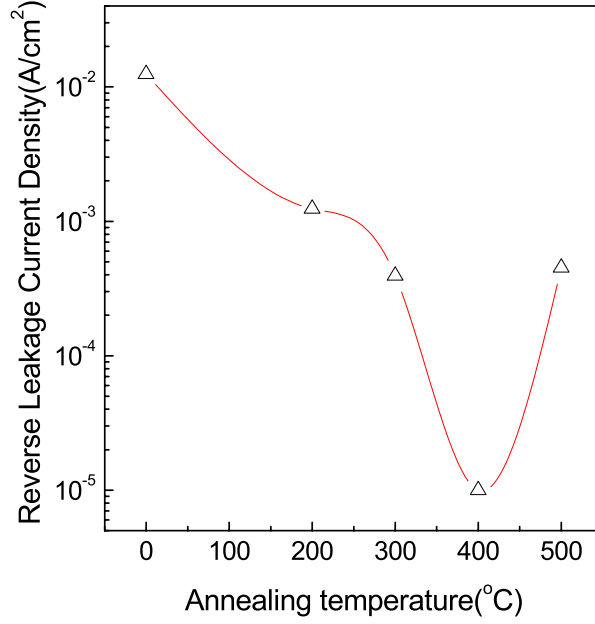
Figure 4.4: The reverse leakage current density measured at -3 V against the annealing temperature.

made that the current-limiting process is the actual transfer of electrons across the interface between semiconductor and metal. The inverse process under reverse bias is analogous to thermionic emission of electrons from a metal into semiconductor with the barrier height ϕ_b. The effects of drift and diffusion in the depletion region are assumed to be negligible. The current voltage characteristics of metal-semiconductor Schottky contact are given according to the thermionic-emission model. From the forward log I-V curves, the ideality factor n, Schottky barrier heights ϕ_b, and saturation current I_s can be obtained in according to following equations:

$$J = J_s\{exp[\frac{q(V - IR_s)}{nkT}] - 1\},\tag{4.4}$$

50

$$J_s = A^*T^2 exp(-\frac{q\phi_b}{kT}) \qquad (4.5)$$

where

$$A^* = \frac{4\pi m^* q k^2}{h^3} \qquad (4.6)$$

A^* is the Richardson constant for thermionic emission except for the substitution of the semiconductor effective mass m^* for the free-electron mass m; it has the value

$$A^* = 1.2 \times 10^6 (\frac{m^*}{m}) \quad m^{-2}K^{-2} \qquad (4.7)$$

provided the conduction band of the semiconductor has spherical constant-energy surface, q is the electron charge, J_s the saturation current density, V the applied voltage, R_s the series resistance, k the Boltsman constant, ϕ_b the effective barrier height, n the ideality factor. The ideality factor n and barrier height ϕ_b can be determined from the intercept and slope of forward $\ln J$ versus V plots using equations
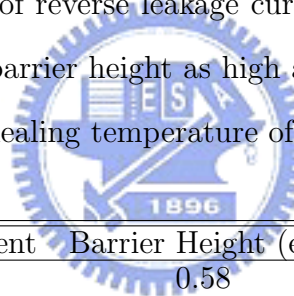
$$n = \frac{q}{kT} \cdot \frac{\partial V}{\partial \ln J} \qquad (4.8)$$

and

$$\phi_b = \frac{kT}{q} \cdot \ln[\frac{A^*T^2}{J_s}] \qquad (4.9)$$

According to thermionic emission model, the Schottky barrier height and ideality factor corresponding to different annealing conditions are summarized in Table 4-3. Earlier I-V measurement[48] had produced p-type Schottky barrier value ϕ_b=0.52 eV with no thermal treatment, essentially in agreement with our result of as-deposited

51

sample. After thermal treatment, these fitting parameters showed that the barrier height increased with increasing annealing temperature between 200 and 400 ^{0}C, but the ideality factor decreased. As the annealing temperature raising to 500 ^{0}C, the barrier height was lower and the ideality factor become larger. Since the cleaved surface of GaSe has no dangling bonds and no surface states, there was no chemical interaction between Au and GaSe. During the annealing process, thermal treatment can offer Au more kinetic energy to react with the surface of GaSe. When the annealing temperature keep on raising to 500 ^{0}C, the poor Schottky performance was obviously presented. This means that this diode structure can not stand a thermal treatment which is above the GaSe surface deterioration temperature for 10 min. at 500 ^{0}C. Additionally, those fitting parameters varied with annealing temperature is also responsible to the results of reverse leakage current. Finally, the optimal rectifying characteristics with the barrier height as high as 0.68 eV and ideality factor of 1.79 were obtained around annealing temperature of 400 ^{0}C.

Annealing Treatment	Barrier Height (eV)	Ideality factor
as-deposited	0.58	3.35
200 ^{0}C/10 min.	0.59	2.10
300 ^{0}C/10 min.	0.62	1.93
400 ^{0}C/10 min.	0.68	1.79
500 ^{0}C/10 min.	0.67	2.10

Table 4.3: The fitting results of IV measurement of the Au/Er:GaSe ([Er] 0.2%) at different anneal temperatures.
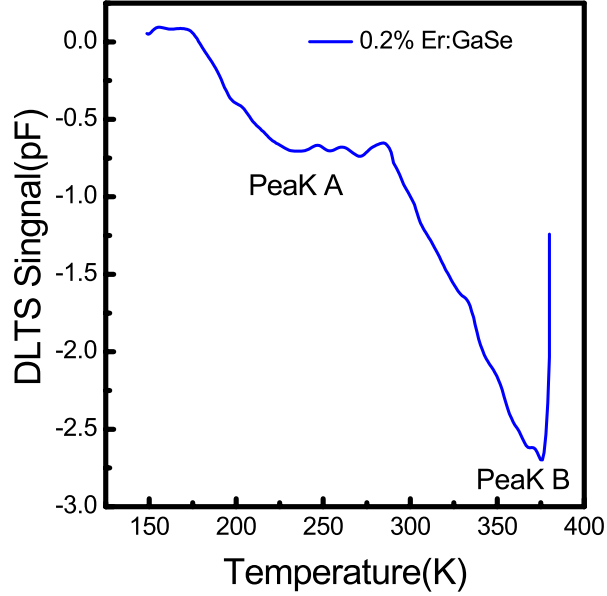
Figure 4.5: DLTS spectrum of 0.2% Er:GaSe.

4.3.4   Deep-level Transient Spectroscopy

DLTS spectra were measured to obtain more information about the trap level and
trap capture cross section in Er:GaSe. Figure 4.5 displays the DLTS spectra from a
0.2% Er:GaSe sample. The applied pulse bias did not exceed the DC bias throughout
the experiments, so only the impurity levels of majority carrier (hole) traps were
determined. Two peaks, A and B, were obtained at temperatures of about 240 and
370 K. The thermal emission rate e_P was related to the activation energy of the trap
level, E_t, and the hole capture cross section, σ_P, by the well-known equation[49]

$$e_P = \sigma_P v_P N_v \exp(-E_t/k_B T_M) \tag{4.10}$$

53

where v_P is the average thermal velocity of holes and T_M is the peak temperature of the DLTS signal. v_P is assumed to vary as $T^{1/2}$, and N_V as $T^{3/2}$. The activation at a given trap level can be determined from the slope of $\ln(e_P/T_M^2)$ vs $1/T_M$. Figures 4.6 (a) and (b) present the Arrhenius plots that correspond to peaks A and B, respectively.
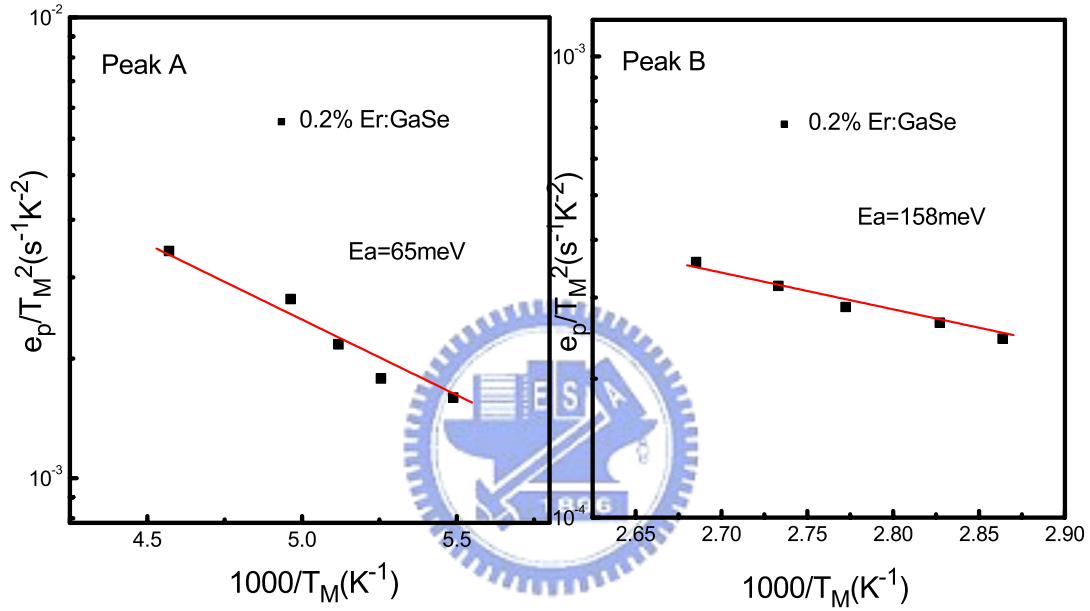
Figure 4.6: Arrhenius plot of e_P/T_M^2 vs $1/T_M$ in peaks A and B.

The solid lines represent least-square fits and the activation energies of both acceptors are 65 meV and 158 meV, corresponding to the trap capture cross section of 2.94×10^{-16} and 5.89×10^{-16} cm^{-2}, respectively. Moreover, the energies 65 meV and 158 meV are quite close to the activation energies of the acceptor levels obtained by measuring the concentration of holes. The trap level, corresponding to peak B

detected by DLTS, at around 158 meV, was not obtained by PL measurement in Ref. [44], suggesting that the trap state acceptor acts as a nonradiative center. This impurity level is consistent with the result of Er-related luminescence and involves energy transfer from GaSe host material to excite the $4f$-shell of erbium.

4.4　Conclusions

The electrical characteristics and Er-related luminescence of Er:GaSe samples were studied using Hall, DLTS and PL measurements. The temperature-dependence of carrier concentration reveals that erbium introduced two acceptor levels with ionization energies of ~ 65 and 158 meV. The measurements of DLTS and of the temperature-dependence of Er-related luminescence indicate that the moderately deep acceptor level of 158 meV is importantly involved in the thermal quenching mechanism, which is associated with the energy back transfer process. Additionally, these acceptor levels could be associated with the substitution of two Ga^{2+} atoms by one Er^{3+} atom or are related to a Ga vacancy via the interstratifying of an Er^{3+} ion at the interlayer site. The temperature-dependence of hole mobility was also analyzed by scattering from homopolar optical phonons and ionized impurities.
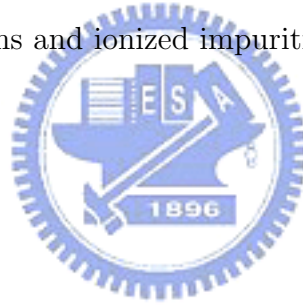
Chapter 5

Theoretical Background of Difference-Frequency Generation

5.1 Retracing Behavior of Phase-matching Angle in GaSe Crystal

In this section we will summarize the principle of mid-infrared generation by difference-frequency generation, since the theoretical consideration have been treated by numerous authors.

When intense electromagnetic waves propagate through a nonlinear optical material, the polarization P induced by the applied electric field E can be expressed as:

$$P(t) = \chi^{(1)}E(t) + \chi^{(2)}E^2(t) + \chi^{(3)}E^3(t) + ... \tag{5.1}$$

where the quantities $\chi^{(1)}$, $\chi^{(2)}$, and $\chi^{(3)}$ are referred the linear, the second- and third-order nonlinear optical susceptibilities, respectively. In the case of three waves parametric mixing, the driving field consists of two distinct frequency components ω_1 and ω_2:

$$E(t) = E_1 e^{-j\omega_1 t} + E_2 e^{-j\omega_2 t} + c.c. \tag{5.2}$$

The time-varying polarizations act as the source for the generation of a new electromagnetic field, as described by the following wave equation based on Maxwell wave equation:

$$\nabla^2 E - \varepsilon_0 \mu_0 \frac{\partial^2 E}{\partial^2 t} = \mu_0 \frac{\partial^2 P}{\partial^2 t} \tag{5.3}$$

Difference-frequency generation is a frequency down-conversion process by the nonlinear polarization $P(\omega_1 - \omega_2) = 2\chi^2 E_1 E_2^*$ which gives rise to a new electromagnetic field at the difference-frequency of two incident waves E_1 and E_2 via χ^2 nonlinear parametric interaction in a nonlinear optical crystal. This process can be schematically shown in Fig. 2.1. A "signal" photon (at frequency ω_s) simulates the break down of a "pump" photon (at frequency ω_p) into "signal" and "idler" photons (at an infrared frequency $\omega_i = \omega_p - \omega_s$) satisfying the laws of conservation of photon energy and momentum. The subscripts s, p, i refer to the signal, pump, and idler (infrared), respectively.

Due to optical frequency dispersion in the refractive index of nonlinear crystals, the interacting waves at different frequencies travel at different velocities (defined as c/n(ω), where c is the speed of light and n(ω) is the frequency-dependent refractive index). The difference in the phase velocities produces a phase difference that accumulates along the length of the nonlinear device. The relative phases of the interacting waves determine the direction of the generated power flow. A phase shift of π is produced over every coherence length, which can lead to a reversal of the

58

energy flow between the driving and generated waves. For efficient frequency conservation, the critical requirement is that the interacting waves must stay in phase along their path through the nonlinear medium. This requirement is usually referred to as phase-matching. The efficiency of nonlinear generation at the frequency ω_i is given by

$$\eta = \frac{2\omega_i^2 d_{eff}^2 L^2 P_s}{\varepsilon_0 c^3 n_i n_s n_p A} sinc^2(|\Delta K|L/2) \tag{5.4}$$

assuming a plane wave approximation, and where K is the wave vector within the nonlinear optical medium and ΔK describes the phase mismatch resulting from unequal phase velocities of the interacting waves; L is the wave interaction length inside the nonlinear materials, P_s is the signal laser power, d_{eff} is the effective nonlinearity, and A is the cross-sectional area of the laser beam. The wave vector mismatch ΔK is given by $\triangle K = K_p - K_s - K_i$. Although many parameters influence the efficiency of nonlinear conversion, the phase-matching condition and the energy conservation are the crucial factors. The phase-matching generally implies a vectorial identity, however, the wave vectors of three interacting waves are parallel in a collinear phase-matching configuration.

$$\omega_p = \omega_s + \omega_i \tag{5.5}$$

$$\frac{\omega_p n(\omega_p, \theta, T)}{c} = \frac{\omega_s n(\omega_s, \theta, T)}{c} + \frac{\omega_i n(\omega_i, \theta, T)}{c} \tag{5.6}$$

here $n(\omega, \theta, T)$ represents refractive index, which is usually a function of wavelength, temperature, and the angle between the optical axis of nonlinear crystal and the wave

vector of the extra-ordinary wave. We usually call θ as the phase-matching angle for an optical parametric process. In the case of GaSe crystal, GaSe belongs to negative uniaxial crystal $(n_o > n_e)$. The refractive index of the extraordinary wave is, in general, a function of θ and can be determined by the equation:

$$n^e(\theta) = n_o\sqrt{\frac{1 + tan^2(\theta)}{1 + (n_o/n_e)^2 tan^2(\theta)}} \tag{5.7}$$

Note that if the polarization states of the three interactive waves are the same, the left-hand side of Eg.(2.6) is always larger than the right-hand side, resulting in no solution for phase-matching condition. In order to fulfill the phase-matching condition, differently polarized waves should be used. Therefore, there are two types of angle phase matching. Type I refers to the situation where the pump and signal waves have the same polarization. In type II phase matching, the two waves are orthogonal polarizations. In this studies, the type I phase-matching was used because of the smaller phase-matching angle, which result in less Fresnel's losses.

5.2 Calculations of Tuning Curves Based on Quasi-phase Matching in PPLN Crystal

Over the last decade there has been a rapid development in quasi-phase matching (QPM) technique. QPM materials have proven to be very valuable for efficient frequency conversion. For example periodically poled $LiNbO_3$ (PPLN), $KTiOPO_4$ (PP-KTP), $RbTiOAsO_4$ (PPRTA), $LiTaO_3$ (PPLT), and QPM-GaAs are commercially available or experimentally investigated. In the QPM scheme, periodic structures are used to achieve phase-matching. In order to offset the accumulated phase mismatch

the signs of the optical nonlinearity of the crystals are modulated along the propagation direction so that the phase is periodically reset by π with half-period equal to the coherence length. Two techniques are involved: (1) electric-field poling ferroelectric materials (such as LiNbO$_3$), and (2) stacking-bonding semiconductor plates (such as GaAs) by rotating alternative wafers. In contrast to birefringent phase-matching, since QPM does not rely on birefringence, it can thus be achieved at any wavelength within the transparency range of the crystal by selecting the modulation period of the nonlinearity grating Γ and it allows a free choice of polarization of the interacting waves, permitting to use the largest nonlinear susceptibility.

According to the original idea of QPM, the phase-matching condition, Eq. (2.6) can be modified to become:

$$\frac{\omega_p n(\omega_p, \theta, T)}{c} = \frac{\omega_s n(\omega_s, \theta, T)}{c} + \frac{\omega_i n(\omega_i, \theta, T)}{c} + m \frac{2\pi}{\Gamma(T)} \tag{5.8}$$

here the parameter Γ presents the period of domain inversion or the $\chi^{(2)}$ coefficient distribution of the nonlinear medium; the integer m stands for the order of QPM. Because of thermal expansion, Γ is usually a function of temperature T. In general, one set of ω_p, ω_s, and ω_i only has a unique period Γ to satisfy the phase-matching condition (Eq. (2.8)) at a temperature. Since the period Γ is well defined after the material process, we can only fine tune the frequency sets by changing temperature of the nonlinear optical crystal in the normal incident collinear configuration or changing the incident angle to slightly modify the effective period Γ.

61

Chapter 6

Difference Frequency Mixing in GaSe Crystal

6.1   Introduction

Nonlinear optical frequency down-conversion by means of a $\chi^{(2)}$ parametric interaction process, such as difference-frequency generation(DFG) and optical parametric oscillation(OPO), can be employed to generate coherent sources at mid-infrared wavelengths in which there exist no convenient direct lasering sources. Coherent sources in the mid-infrared ray are of prime importance for molecular spectroscopy, eye-safe medical instrumentations, radar and remote sensing of atmospheric constituents, and numerous military applications. In order to generate high power IR coherent source, suitable nonlinear optical materials with large magnitude of second-order susceptibilities are considerable. Among different classes of second-order nonlinear optical materials, GaSe crystal has comparatively lower absorption coefficients and appropriate amount of birefringence for phase-matching($\Delta n \approx 0.35$ at 1 μm). On the negative side, GaSe is a soft, layered material that can be cleaved only along the 001 plane (z-cut orientation); it also provides a large walk-off angle. Recently, Y.J. Ding et

al.[18] demonstrated a continuous-tunable and coherent radiation in the extremely-wide range of 2.7-38.4 μm and 58.2-3540 μm based on different-frequency mixing in GaSe crystal for the first time. Such amazingly tunable range in Ding's results proved that GaSe possesses great potential for nonlinear frequency down-conversion. Therefore, using GaSe crystal to generate infrared light source based on parametric interaction process is a interesting subject.

During the past two decades, extensive experimental studies had been carried out in this field of research in the continue-waves, nanosecond, picosecond and femtosecond regime applied with GaSe crystals. In application of applied spectroscopy such as biomedical diagnostics and chemical identification, high spectral purity, wide wavelength tunability and appropriate output power are considered. For these experimental applications the nanosecond time domain is optimal, because it offers a high spectral resolution and output average power of the order of few watts. Another attractive application is the studies of intersubband lifetimes and free carrier effects in semiconductor quantum wells. Electron intersubband lifetimes in the picosecond regime can be measured by using a pump-probe far-infrared technique. In order to achieve a population inversion between the second excited subband, the estimated threshold pump power is in the region of 100 kWcm^{-2}. Consequently, IR picosecond pulse is suitable for the time resolved investigations of the dynamics of infrared states. Besides, high output energies in the microjoule range are also essential to achieve substantial excess populations. In this chapter, therefore, both the nanosecond and picosecond radiations in the mid-infrared based on DFG in GaSe were studied. Additionally, N.B. Singh et al.[50] reported that the silver gallium selenide doped GaSe crystals possessed a high nonlinear coefficient of 75 pm/V resulting in

63

significant increase of the d^2/n^3. This dopant in GaSe enhanced the intrinsic value of the nonlinear coefficient. In the case of the indium doped GaSe,[51] it showed the improvements in second-harmonic generation efficiency and the mechanical properties. Both improvements are ascribed to better crystal quality by means of doping indium. Consequently, the variation in nonlinear coefficient is possibly the origin of crystal quality and doping impurity. The erbium doping in GaSe causing the substitution or interstitial were interesting. In addition to the investigation on the optical and electrical properties of erbium doped GaSe crystals, the nonlinear optical property will be examined in this chapter.

In this thesis, we successfully demonstrated that our GaSe crystals can be used to generate mid-infrared sources with both pulse durations of 5 ns and 5 ps, respectively, from different-frequency mixing systems. In the nanosecond regime, the signal and idler waves output from Nd:YAG-laser-pumped PPLN OPO were collinear mixing in GaSe crystal to generate tunable radiation from 4.35 to 14.25 μm. The conversion efficiency and tuning characteristics of different-frequency mixing were discussed in detail. In the picosecond regime, the picosecond infrared pulses were generated by using the 1.064 μm pump and signal pulses of a parametric device based on a 10 Hz Nd:YAG amplifier system. Besides the characteristics of output picosecond pulses, the effect of erbium doped GaSe crystals in this system of different-frequency mixing were also discussed.

6.2 DFG of Output Waves from a PPLN Optical Parametric Oscillator in a GaSe Crystal

6.2.1 Experiment

A scheme of the experimental setup is shown in Fig. 6.1. A New Wave Minilaser, Series II (Nd:YAG) serves as the pump source, which generates pulses of wavelength 1.064 μm with a duration $\approx$ 7 ns and a repetition rate of 17 Hz. The pump beam diameter was compressed from 2.7 to 1 mm by a telescope. Both the lenses forming the telescope are antireflection-coated at the pump wavelength. A maximum pump energy of 10.5 mJ can be obtained from the pump source, which corresponds to a peak intensity of $\approx$175 MW/cm^2. The OPO resonator was a linear cavity with flat mirrors, selected to resonate at the signal frequency as a singly resonant oscillator (SRO). The PPLN crystal, having a grating period of 31 μm with dimensions 40 mm$\times$35 mm$\times$31 mm, is placed in a temperature controlled oven. Detailed description of the fabrication process of the PPLN sample used in this experiment can be found in Refs. [52] and [53]. The cavity mirrors M1 and M2 are broadband dielectric-coated for the signal wave; M1 is 99% reflective for the signal wave in the range of 1.72 to 2 μm, and the output coupler M2 is 70% reflective at signal wavelengths (1.68 to 2 μm). The cavity physical length was adjusted to 6 cm. The PPLN crystal end faces were antireflection-coated for the pump wavelength.

6.2.2 Results and Discussion

The PPLN OPO produced output wavelength tunable from 1.71 to 2.81 μm with the crystal temperature varying from 40 to 175^{0}C. The measured tuning curve, as shown
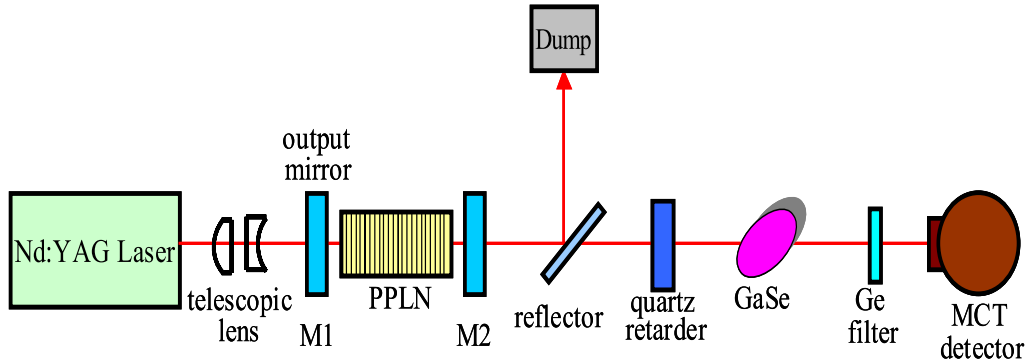
Figure 6.1: Schematic diagram of the experimental setup.

in Fig. 6.2, matches well with the calculated Sellmeier fit. The output characteristics and oscillation threshold of the OPO were also determined by keeping the oven temperature of the crystal at 140^0C throughout the experiment to avoid photorefractive damage. The oscillation threshold was found to be 0.65 mJ at the signal wavelength of 1.85 μm.

The linewidth of the signal is shown in Fig. 6.3. As the pump pulse width was ≈7 ns, multiple-pass gain did not have a significant effect on linewidth narrowing, as compared to the linewidth output from a single-pass gain.[54] Linewidth was measured while operating the OPO at pump power of 1.5 times above threshold. Widening of the linewidth has also been found while increasing the pumping intensity. The beam quality of the OPO output was measured, and we found M^2≈8 in our experiment. Beam quality and linewidth are two most important factors to be considered for generating OPO output beams in a nonlinear crystal.

The PPLN OPO generates two beams with wavelengths in the ranges 1.71 to 1.98
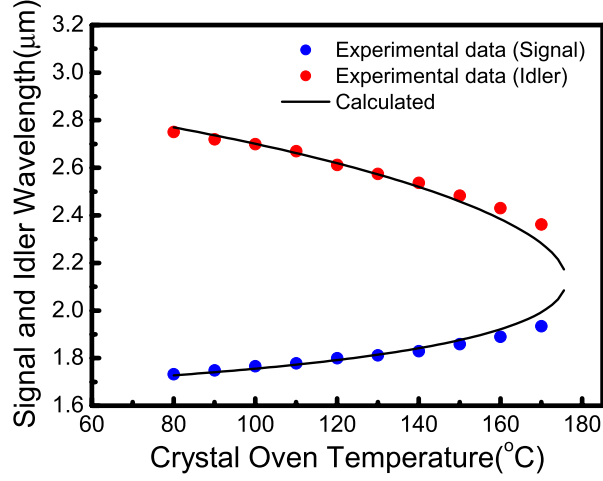
Figure 6.2: Temperature tuning characteristics for the 1.064 μm pumped PPLN OPO with 31 μm period.

μm and 2.81 to 2.30 μm for the signal (λ_s) and the idler (λ_i) waves, respectively, which were focused by a quartz lens with focal length f=25 cm onto a GaSe crystal. These waves were mixed in the GaSe crystal for difference-frequency generation in the mid-IR,successfully produced a third wave with a wavelength tunable from 4.35 to 14.25 μm. The GaSe crystal used in the experiment was 3 mm long, having a semicircular cross section ≈4 mm in radius. The normal to the entrance face of the crystal was found experimentally by adjusting the crystal so that a He-Ne laser beam passing through a pinhole in a white card was reflected back along its incoming path. The effective nonlinear coefficients depend on the phase matching (θ) and azimuthal (ϕ) angles in the following way[55]:

67
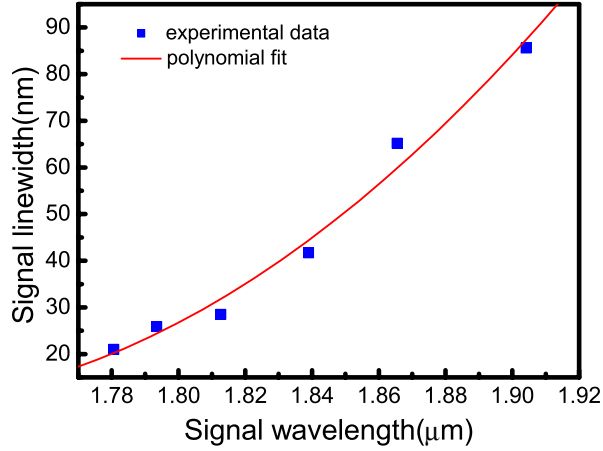
Figure 6.3: Linewidth of the PPLN OPO as a function of signal wavelength.

$$TypeI(0 \longrightarrow e - o) : d_{eff} = -d_{22} \cos\theta \sin 3\phi \tag{6.1}$$

$$TypeII(e \longrightarrow e - o) : d_{eff} = -d_{22} \cos^2\theta \cos 3\phi \tag{6.2}$$

The highest effective nonlinearity is achieved by selecting azimuthal angles ϕ determined by $| \sin 3\phi |= 1$. Rotation angles of the GaSe crystal were calculated using the dispersion relation of Ref. [56] to match difference-frequency phase condition over the OPO tuning range. The calculated tuning curve is shown in Fig. 6.4. If the signal and idler waves from OPO have the same polarization, a retarder is necessary to rotate two polarizations to be orthogonal as required by the phase-matching conditions. In our experiment, we employed type-I phase matching because its required phase-matching angle is less than that for type II. Since the azimuthal angle ϕ was unknown

68

to us, optimum DFG mixing was achieved by tuning the signal and idler wavelengths from OPO, and rotating the angle θ of GaSe crystal for the phase-matching condition (θ to the vertical) and azimuthally angle ϕ until maximum DFG power was obtained. From Fig. 6.4 the experimental data matches to the calculated tuning curve with a little shift, probably due to the measurement error. For the entire tuning range from 4.35 to 14.25 μm the crystal internal angles, were changed between 11^0 and 12.5^0, requiring an external angle of incidence between 31.5^0 and 36.5^0; a 5^0 angular rotation sufficed for tuning.
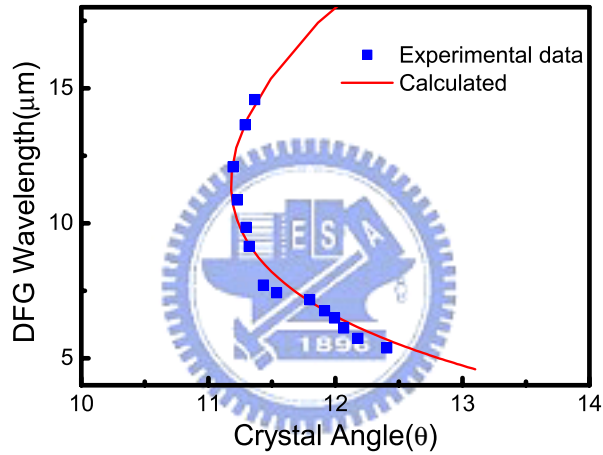
Figure 6.4: DFG tuning characteristics of the GaSe crystal for mixing of PPLN OPO waves.

The mid-IR pulses were separated from the OPO pulses by two dielectric-coated Ge filters and detected with a liquid-nitrogen-cooled HgCdTe detector. The DFG power was also measured by a pyroelectric detector and was found to have a maximum of ≈ 10 μJ at ≈ 7 μm, for a sum energy of signal and idler waves of 2.7 mJ. The generated DFG power was much lower than the estimated power of ≈ 85 μJ. One of

69

the reasons for the poor conversion efficiency was high reflection loss from the crystal surfaces. The crystal was not antireflection-coated, and the high refractive index of GaSe crystal causes the loss. Considering the reflection losses and linear absorption, the conversion efficiency was estimated to be reduced to $\approx$47%. Poor surface quality of the sample crystal adds to the losses too.

The acceptance linewidth in the three-wave interaction for the whole tuning range varies, and has a value of 23 nm (for a 3-mm long GaSe crystal) at $\lambda_s \approx 1.85$ μm, which is larger than the experimentally obtained OPO signal linewidth of 14.5 nm. The effect of beam divergence was also taken into account for the mixing process; the beam divergence of the OPO output beam was $\approx$ 6 mrad, and the calculated acceptance angle for the GaSe crystal was $\approx$ 4 mrad at $\lambda_s \approx 1.85$ μm. The narrow acceptance angle of GaSe crystal also contributed to the reduced conversion efficiency.

6.3 Tunable and Coherent Picosecond Radiation in the Mid-infrared by DFG in GaSe

6.3.1 Experiment

The experimental system is depicted in Fig. 6.5. The pump source is a 1.064 μm Nd:YAG laser and the signal source is a $\beta - BaB_2O_4$(BBO)-based OPO. The Nd:YAG fundamental pulses at 1.064 μm had a pulse duration of 20 ps and a repetition rate of 10 Hz. The OPO, which was pumped with the 355 nm line from a Nd:YAG/THG(third harmonic generation) laser, can generate an idler with wavelength tunable in the range of 1.1-1.8 μm with a pulse duration of 5 ps. The pulse energy of the Nd:YAG laser is attenuated to 750 μJ and the idler waves of OPO are varied between 35 and 50 μJ for each pulsebefore incidence. The beam spot size for pump beam was measured about 1.6 mm, which corresponds to a maximum peak intensity of 1.7 GW/cm^2. The signal beam from the OPO laser was combined parallel with the pump beam (collinear configuration) using a polarizing beam splitter. The polarization directions of pump and signal lights were vertical and horizontal, respectively. The temporal overlap of the two incident beams was adjusted using an optical delay line. The GaSe crystal was mounted on a precise rotation stage.

In this part of experiment, we use pure and erbium doped GaSe crystals having a thicknesses of 6.5 mm, and a cleaved ellipsoidal face with the lengths of the major and minor axes to be 15 and 10 mm, respectively, and with no antireflection coatings on them. Different concentration of erbium doped samples were also employed in this study. The generated mid-IR radiation was detected by a cryogenically cooled MCT detector and a bolometer combined with a digital oscilloscope. A Ge filter
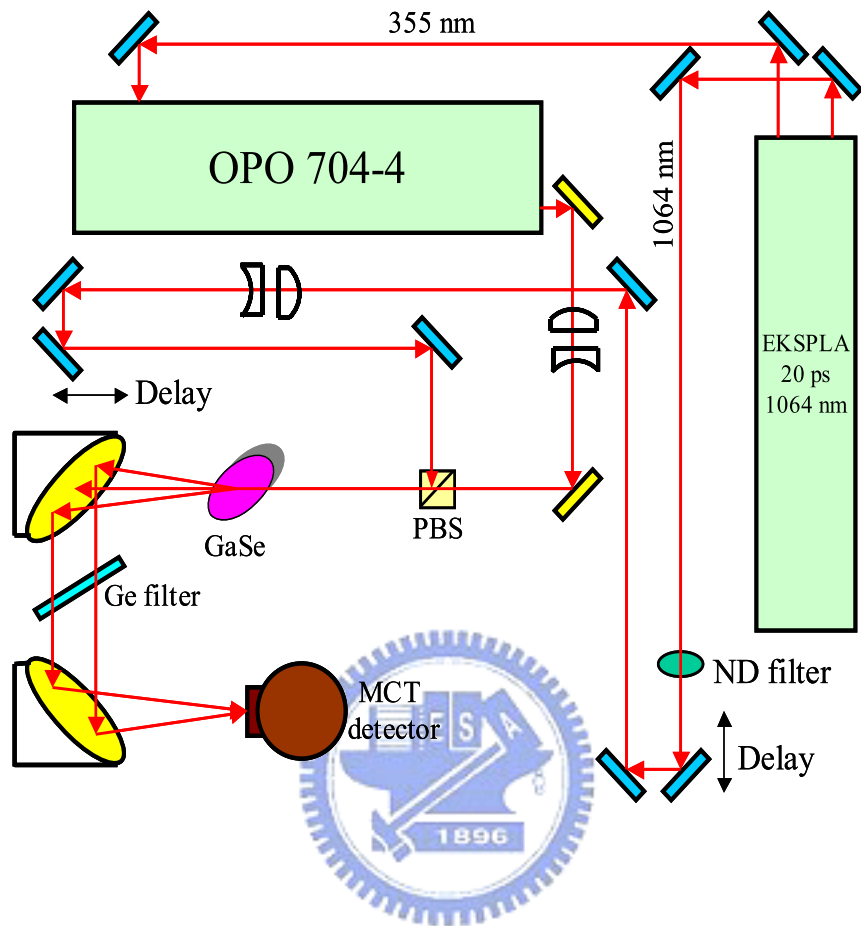
Figure 6.5: Experimental system for generation of tunable infrared picosecond pulses.

was used to block near-infrared pump radiations. This filter completely eliminates all the pumping wavelengths without blocking any IR output wavelength. The pulse energies obtained by us are correcting for the Fresnel reflections and the transmittance of Ge filter. The pulse energy of the generated mid-IR radiation was measured by a pyroelectric detector and calibrated a MCT detector.

6.3.2 Results and Discussion

First we examine the tuning curves of the nonlinear crystals GaSe based on DFG. Figure 6.6 shows the external phase matching angle as a function of the idler wavelength for difference frequency with a pump wavelength of λ=1.064 μm. The circle-points indicate the experimental results, and the solid-line is theoretical calculation from refractive index data in Ref.[56]. Meanwhile, azimuthal angle ϕ is optimized for type I phase matching, which exhibits smaller phase matching angles, walk-off, and higher efficiency than type-II. Tunable and coherent picosecond pulses in the range of 2.4-30 μm are achieved based on type-I DFG in GaSe. Wavelength tuning does not require readjustment of the time delay between pump and signal pulses. We observe good agreement between the experimental data and the theoretical calculation curve. The external angles are between 34^0 and 80^0 in z-cut crystals, corresponding to DFG wavelength from 2.5 to 30 μm. The high nonlinearity of GaSe allows an efficient generation of infrared pulses even though the considerable reflection losses from the large angle occur. Besides, the results of tuning curves in 0.2% and 0.5% doped Er:GaSe crystals are also in agreement with the theoretical calculation curve. It significantly appears that the refractive index dose not change dramatically in the erbium doped crystals. Therefore, the dispersion relations of Ref.[56] are still applicable for erbium doped GaSe crystal.

The measured infrared output pulse energies in undoped, 0.2%, and 0.5% Er:GaSe crystals at different infrared wavelength are shown in Fig. 6.7. These values are obtained after correcting for the transmittance of the Ge filter. The pulse energies range between a maximum of about 5 μJ and 0.1 μJ, corresponding to the wavelength of 3.5 μm and 20 μm, respectively. The three GaSe crystals show the almost similar
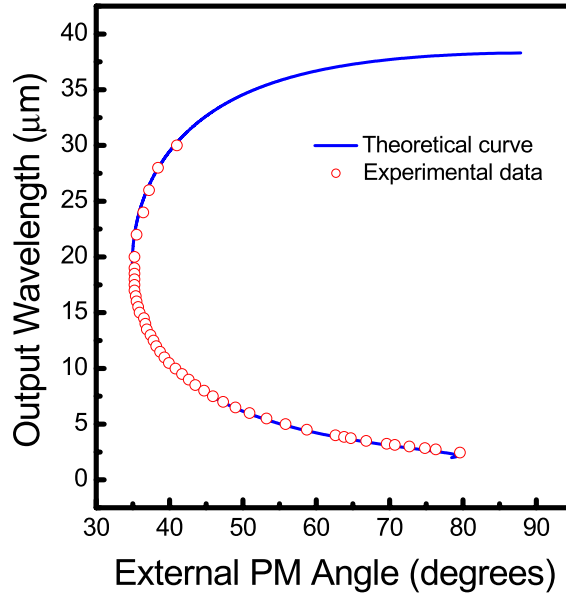
Figure 6.6: Type-I DFG output wavelength vs external phase-matching(PM) angle

maximum output, which are about 5 μJ around the wavelength of 3.5 μm. The maximum photon conversion efficiency greater than 8% is achieved at a wavelength of 3.5 μm. Our photon conversion efficiency is higher than the Dahinten's result of 2% [57], but much lower than the maximum efficiency of 50% that was reported by Finsterbusch et al.[58]. Experimentally, we observed the transmittance of about 59% while the pump beam with the intensity of 1.5 GW/cm^2 at 1.064μm through GaSe crystal. After taking out the reflected losses and linear absorption, there are still much losses in GaSe. The reason could be ascribed that the two-photon absorption (TPA) occurs when the laser photon energy is larger than half the band gap of GaSe crystal, and can set the limit to the performance of photon conversion efficiency.

TAP, which have been reported the value of β=6.3×10^{-9} cm/W at the wavelength of 1.064μm, would produce the nonlinear absorption losses in GaSe while intensity of incident beam up to the order of GW/cm^2.

Keeping on tuning to shorter infrared wavelengths is limited by two possible reasons in this experiment. On the one hand the increasing angle of incidence of the GaSe crystals results in a reduced free aperture and a higher reflection loss. On the other hand the pulse energy of signal wave from OPO system is lower as tuning to the longer signal wave. As tuning to the longer infrared wavelength, the results from using the erbium doped GaSe crystals indicated broader tuning range and slightly higher output pulse energy. According to IR transmission from the undoped and 0.5% Er:GaSe crystals, as shown in Fig. 6.8, the transmittance of the erbium doped GaSe crystal was compared highly with the one of undoped crystal while the output wavelength was above 15 μm. Although the difference of output pulse energy between two crystals is not too obvious, therefore, the slightly higher output pulse energy in erbium doped crystal could be ascribed to higher transmittance for longer wavelength. From the results of DFG experiment, unfortunately, the doping effect resulting in variation of effective nonlinear coefficient can't display. The reason could be that the difference-frequency mixing requires two input laser source. As aligning two laser beams collinearly, the deviation of two beams, such as misalignment and different divergence angle, always arose in the DFG experiment. The most commonly used method to determine the effective nonlinear coefficient is second-harmonic generation(SHG), because SHG benefits from well-established focused beam theories for type-I and type-II interactions. Subsequently, we will use the picosecond infrared light source generated by our DFG system as a pump beam to achieve the frequency

75

doubling in the erbium doped GaSe crystals.

We measured the SHG efficiency for erbium doped GaSe samples to determine the effects of doping on the nonlinear coefficient. The previous DFG system tuned to the wavelength of 6 μm was used, as shown in Fig. 6.9. The output of the DFG system had a pulsed width of 5 ps, and the pulse energy was available up to $\sim 1\mu$J. We determined optimum position by varying the orientation and position of the crystal until maximum SHG output was observed. The pulse energy in both the fundamental beam at 6 μm and the doubled frequency was measured with MCT detector. A 1-mm-thick glass plate was used to separate the two wavelengths, and the absorption of the plate was factored into the efficiency measurement.

Type I phase matching was used with an ordinary wave input and obtained an extraordinary output wave. The external phase-matching angle of 30.18^0 was adjusted by means of dispersion relations of GaSe. As a function of the input pulse energy, the measured efficiencies of undoped and erbium doped GaSe crystals are displayed in Fig. 6.10. The slope of the efficiency data was also used to determined the effective nonlinear optical coefficient for both crystals. The extracted effective nonlinear coefficient K, using the focused Gaussian beam theory of Boyd and Kleinman, combined with both focusing and double refraction effects can be determined. The theoretical second-harmonic power P_2 is related to K the following equation by

$$P_2 = K P_1^2 L k_1 h(B, \xi) \tag{6.3}$$

where P_1 is the fundamental input power; L is the interaction length; $k_1 = 2\pi n/\lambda_0$, with n being the index of refraction of the input beam; and $h(B, \xi)$ is the Boyd and

76
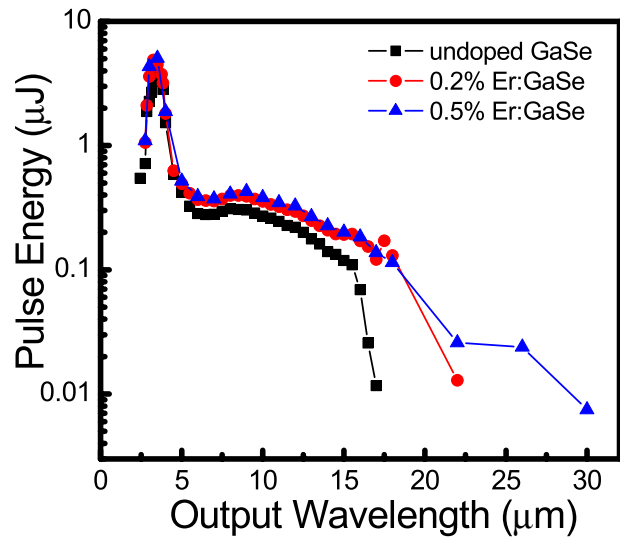
Figure 6.7: Type-I DFG pulse energy vs output wavelength
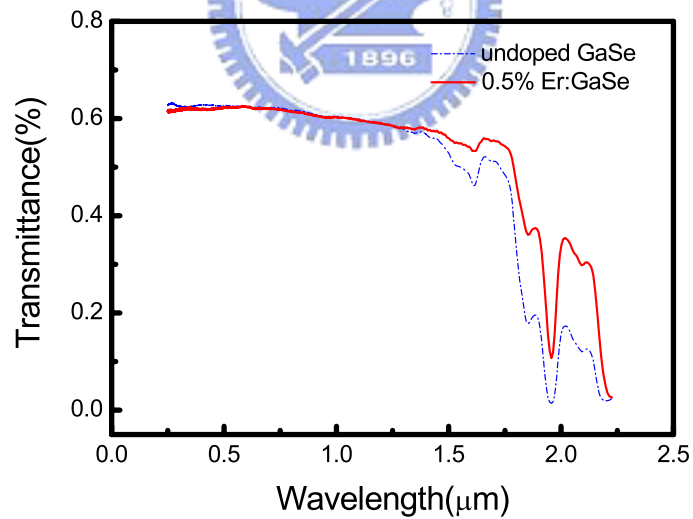
Figure 6.8: Infrared transmission of undoped and 0.5%Er:GaSe crystals

77
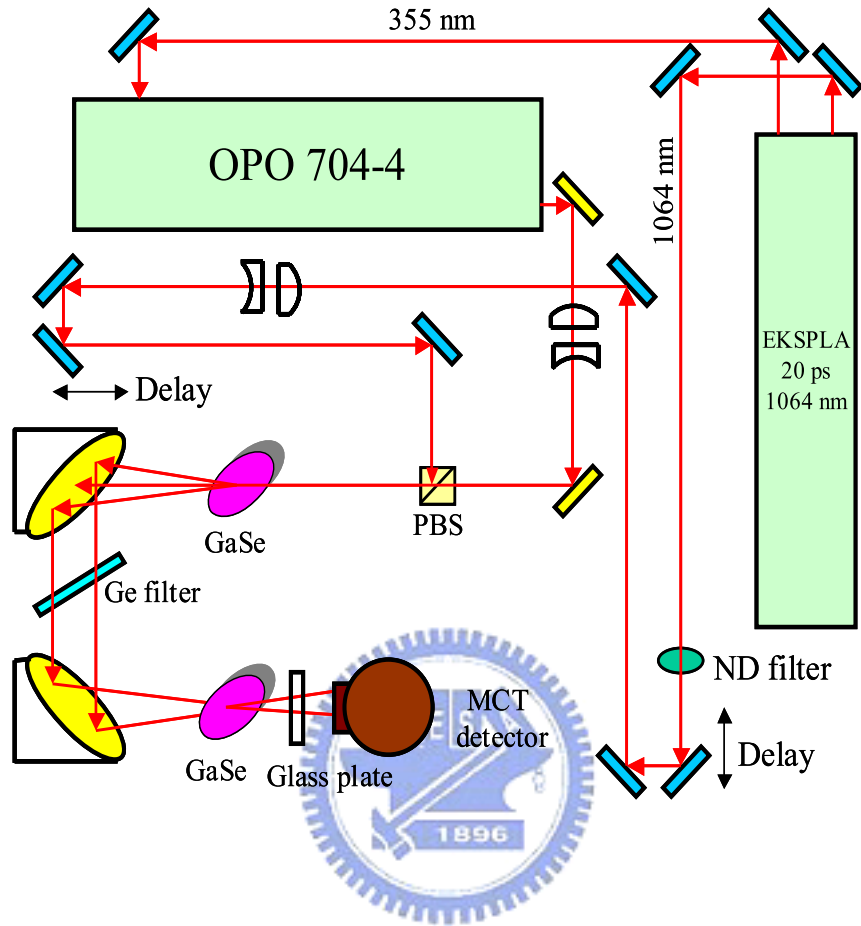
Figure 6.9: Experimental system for SHG.

Kleinman efficiency factor. The double refraction parameter is $B = (\rho/2)(k_1 L)^{1/2}$, where ρ is the walk-off angle between the phase and the power-flow directions. A walk-off angle of 3.4^0 was used, which is the predicted value when the Sellmeier equations are used at the predicted phase-matching angle. The focusing parameters $\xi = L/b$, where b is the length for confocal configuration over which the beam diameter is less than $2^{1/2}\omega_0$. It is given by $b = k_i \omega_0^2$, and the efficiency scaling constant in mks units is

$$K = 8\pi d^2/(c\epsilon_0 n^3 \lambda_0^2) \tag{6.4}$$

where ϵ_0 is the permittivity of free space, c is the vacuum speed of light, and d is the effective nonlinear coefficient in meters per volt.

The measured nonlinear conversion efficiency is the total energy of second-harmonic signal compared with the fundamental pulsed energy and is given by $\eta = \int P_2 dt / \int P_1 dt$, where the integrals are over the temporal duration of the pulse. One can relate this efficiency to the time-independent Boyd and Kleinman theory by measuring the fundamental pulse shape and integrating Eq. 6.3 over time. The result is

$$\eta = KLk_1 h(B,\xi) \int P_\lambda^2 dt / \int P_\lambda dt \tag{6.5}$$

so that by measuring the temporal pulse shape of the fundamental we can relate the experimental conversion efficiency to the theoretical.

Using Equations. (6.3)-(6.5), along with the measured pulse shape, we calculated the effective d_{eff} coefficient by matching the theory to the data. The nonlinear coefficient d_{eff} values of 44.5 pm/V and 55.3 pm/V were determined for the undoped and erbium doped crystals, respectively. The variation in d_{eff} value could be ascribed to crystal quality[51] and impurity doping effect[50]. According to the structural analysis, both the GaSe crystals that were used in this experiment showed the similar crystal quality. It means that the erbium doped in GaSe did not strikingly improve crystal quality like the case of indium doping. But the effective nonlinear coefficient
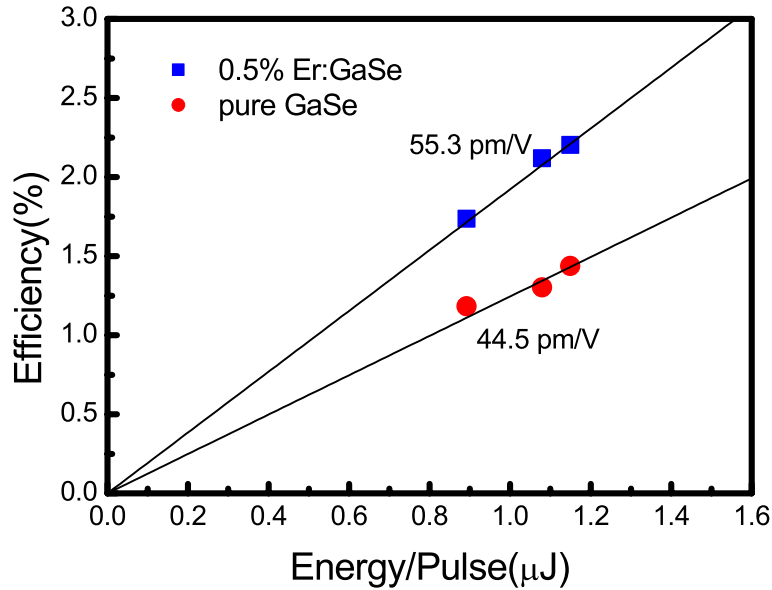
Figure 6.10: SHG in GaSe crystals with the measured d_{eff} values.

d_{eff} is obviously enhanced due to doping erbium elements. The reason has been speculated that the substitution of one Er^{3+} atom for one pair of Ga^{2+} atoms or Er^{3+} ions interstitial at interlayer sites in the unit cell possibly led to the variation in structural symmetry.

6.4 Conclusions

We have reported on the operation of a Nd:YAG-pumped periodically poled LiNbO$_3$ OPO and on difference frequency mixing of the OPO output waves to produce tunable mid-IR from 4.35 to 14.25 mm. The oscillation threshold and slope efficiency of the OPO were 0.65 mJ and 25%, respectively. Because there was no linewidth-narrowing

element in the OPO cavity, the linewidths of the signal and idler wave were large, especially close to the point of degeneracy. The difference-frequency-mixing efficiency was less than the calculated value, mainly due to high reflection loss, poor surface quality, and OPO beam divergence. As the OPO output beam linewidth becomes wider near the degenerate point, the acceptance linewidth will lead to a significant further reduction in the efficiency for longer wavelengths. The effect of OPO output beam divergence plays a less important role regarding the conversion efficiency than do the reflection loss and surface quality, because the GaSe crystal was only 3 mm long.

Besides, we also report an all-solid-state laser system which generate picosecond infrared pulses with duration 5 ps tunable in the range of 2.4-30 μm. Generally, energies of several microjoule are obtained with a maximum of $\sim$5 μJ at wavelength of 3.5 μm, corresponding to photon conversion efficiency of 8%, in undoped and erbium doped GaSe crystals. The conversion efficiency is limited by TPA resulting in mainly internal losses. The infrared picosecond light source were also used to measure the nonlinear coefficient d_{eff} values of GaSe crystals based on SHG technique. GaSe doped erbium showed a d_{eff} coefficient of 55.3 pm/V, which is larger than the one of undoped crystal. The improvement of d_{eff} coefficient could be due to he substitution of one Er^{3+} atom for one pair of Ga^{2+} atoms or Er^{3+} ions interstitial at interlayer sites.

Chapter 7

Conclusions

The central interest of this work was the investigation on the growth of centimeter size GaSe crystals and the characteristics of erbium doped GaSe crystals. The major studies are taken concern of the optical and electrical properties of the erbium doped GaSe. Additionally, using GaSe crystal to generate mid-infrared coherent source based on parametric interaction process was demonstrated. All the results and discussions are summarized as follows:

The centimeter size GaSe single crystals were grown by means of the non-stoichiometric mixture and quartz tube with a capillary, which were used to overcome the volatilization of selenium and reduce the number of nucleation, respectively. According to structural analysis, the pure and erbium doped GaSe crystals showed good crystal quality. In the analysis of component, the erbium concentration were three order magnitude lower than the initial erbium concentration. The result was not clear that the remaining amounts of erbium were incorporated into the crystal or segregated during crystal growth.

From the analysis of optical properties, the luminescence spectra of Er-doped GaSe appear to be affected by the dopant of erbium. The impurity level at $\sim$2.064 eV is

observed and located at ~64 meV above the valence band in both the as-grown and the annealed Er doped GaSe crystal. The emission band at 2.032 eV might be due to the one-LO-phonon replica of the band-impurity recombination at 2.064 eV. The emission bands at 2.103 eV and 2.093 eV are ascribed to structural defects based on the luminescence intensities varying as temperature. Additionally, the infrared luminescence and transmission spectra which have arisen from the intracenter transitions of erbium ions have been observed at ~0.81, 0.99, and 1.54 μm, respectively. The annealing process under excess Se atmosphere at 600 ^{o}C for 72 hours can enhance the crystal to have more active erbium ions. The deep accepter level that located at 162 meV above the valence band was believed to involve the thermal quenching of Er-related luminescence.

In the case of electrical analysis, Hall measurement results show the room temperature hole concentration of order of 10^{17} in Er-doped GaSe samples while their mobility is in the range of 22-34 $cm^2/V \cdot s$. Two acceptors model, in which one acceptor level is found to locate at about 65 meV above the valence band and the other one is at ~158 meV, was explained. Furthermore, the shallow acceptor level plays the role both in contributing free hole carriers and acting as a radiative center and the deep one is a nonradiative center which is responsible for the quenching behavior of Er related luminescence. The temperature dependence of hole mobility can be interpreted by combining the homopolar optical phonon and ionized impurity scatterings.

An optical parametric oscillator(OPO) based on periodically poled lithium niobate pumped by a Nd:YAG laser was demonstrated. Combined signal and idler pulse output from OPO with a maximum energy of 2.7 mJ, which corresponds to a slope

efficiency of 25% have been achieved. The tuning range is 1.71 to 1.98 μm for the signal wave and 2.81 to 2.30 μm for the idler wave. The signal and the idler waves are tuned and difference-frequency mixed in a GaSe crystal to produce tunable mid-IR from 4.35 to 14.25 μm. The DFG efficiency was less than the calculated value, mainly due to high reflection loss, poor surface quality, and OPO beam divergence.

Finally, we also demonstrated the infrared light source that provides picosecond pulses on microjoule energy level, widely tunable in the 2.4-30 μm wavelength range with pulse durations $\sim$5 ps. The energies of several microjoule are obtained with a maximum of $\sim$5 μJ at wavelength of 3.5 μm, corresponding to photon conversion efficiency of 12%. This picosecond light source was applied to evaluate the nonlinear coefficient (d_{eff}) of crystals GaSe doped with erbium based on second harmonic generation. The variation in the d_{eff} values between undoped and erbium doped GaSe could be probably ascribed to the effect of erbium doping, which resulted in substitution or interstitial of Er atom in GaSe unit cell.
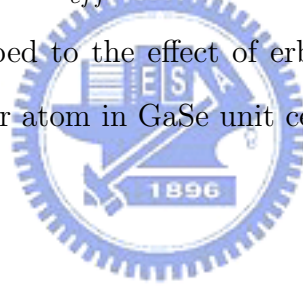
Bibliography

[1] S. Shigetomi, T. Ikari, and H. Nakashima, J. Appl. Phys. **69**, 7936(1991)

[2] S. Shigetomi, T. Ikari, and H. Nakashima, J. Appl. Phys. **74**, 4125(1993)

[3] V. Capozzi, Phys. Rev. B **28**, 4620(1983)

[4] S. Shigetomi, T. Ikari, and H. Nakashima, J. Appl. Phys. **76**, 310(1994)

[5] S. Shigetomi, T. Ikari, and H. Nakashima, Physica Status Solidi (a) **160**, 159(1997)

[6] J. F. Sanchez-Royo, D. Errandonea, A. Segura, L. Roa, and A. Chevy, J. Appl. Phys. **83**, 4750(1998)

[7] G. Micocci, A.Serra, and A. Tepore, J. Appl. Phys. **82**, 2365(1997)

[8] G. Micocci, A.Serra, and A. Tepore, J. Appl. Phys. **81**, 6200(1997)

[9] B. Guurbulak, M. Yildirim, S. Tuzemen, H. Efeoglu, and Y.K. Yogurtcu, Phys. Status Solidi **83**, 2030(1998)

[10] B.G. Tagiev, G.M. Niftiev, and S.A. Abusov, Phys. Solid State A **83**, K61(1984)

[11] A.Sh. Abdinov, R.F. Babaeva, R.M. Rzaev, and G.A. Gasanov, L Nuovo Cimento **40**, 660(2004)

[12] C.D. Kim, K.W. Jang, and Y.I. Lee, Solid State Commun. **130**, 701(2004)

[13] K. L. Vodopyanov and V. G. Voevodin, Opt. Commun. **114**, 333(1995)

[14] K. L. Vodopyanov and V. Chazapis, Opt. Commun. **135**, 98(1997)

[15] R. A. Kaindl, M. Wurm, K. Reimann, P. Hamm, A. M. Weiner, and M. Woerner, J. Opt. Soc. Am. B **17**, 2086(2000)

[16] R. S. Putnam and D. G. Lancaste, Appl. Opt. **38**, 1513(1999)

[17] W. Shi, Y. J. Ding, N. Fernelius, and K. Vodopyanov, Opt. Lett. **27**, 1454(2002)

[18] W. Shi and Y. J. Ding, Appl. Phys. Lett. **84**, 1635(2004)

[19] T. Tanabe, J. Nishizawa, K. Suto, and T. Sasaki, J. Phys. D **37**, 155(2004)

[20] T. Ishiyama, S. Nawae, T. Komai, Y. Yamashita, Y. Kamiura, T. Hasegawa, K. Inoue, and K. Okuno, J. Appl. Phys. **92**, 3615(2002)

[21] A. J. Steckl and J. Heikenfeld, IEEE Tran. Electron Devices **49**, 557(2002)

[22] W. S. Lee, N. O. Kim, and B. I. Kim, J. Mater. Sci. Lett. **15**, 1644(1996)

[23] B. G. Tagiev, F. S. Aidaev, and T. M. Abbasova, Solid State Commun. **66**, 233(1988)

[24] V. L. Cardetta, A. M. Mancini, C. Manfredotti, and A. Rizzo, J. Crystal Growth **17**, 155(1972)

[25] T. Ishii and N. Kambe, J. Crystal Growth **76**, 489(1986)

[26] A. Castellano, Appl. Phys. Lett. **48**, 298(1986)

[27] G. D. Gusinov and A. I. Rasulov, Phys. Status Solidi **18**, 911(1966)

[28] N. B. Singh, D. R. Suhre, V. Balakrishna, M. Marable, and R. Meyer, Prog. Crystal Growth and Charact. **37**, 47(1998)

[29] A. Mercier, E. Mooser, and J. P. Voitchovsky, Phys. Rev. B **12**, 4307(1975)

[30] V. Capozzi and M. Montagna, Phys. Rev. B **40**, 3182(1989)

[31] T. Schmidt, K. Lischka, and W. Zulehner, Phys. Rev. B **45**, 8989(1992)

[32] J. P. Voitchovsky and A. Mercier, IL Nuovo Cimento **22B**, 273(1974)

[33] G. B. Abdullaev, G. L. Belenkii, E. Yu. Salaev, and R. A. Suleimanov, IL Nuovo Cimento **38**, 469(1977)

[34] V. Capozzi, Phys. Rev. B **23**, 836(1981)

[35] J. F. Sanchez-Royo, A. Segura, A. Chevy, and L. Roa, J. Appl. Phys. **79**, 204(1996)

[36] S. Shigetomi, T. Ikari, and H. Nakashima, Jpn. J. Appl. Phys. **35**, 4291(1996)

[37] S. Shigetomi, T. Ikari, and H. Nakashima, Phys. Status Solidi (a) **185**, 341(2001)

[38] U. K. Saha and H. J. Lozkowski, Mater. Res. Soc. Symp. Proc. **442**, 285(1996)

[39] A. Taguchi and K. Takahei, J. Appl. Phys. **79**, 4330(1996)

[40] A. Segura, F. Pomer, A. Cantarero, W. Krause, and A. Chevy, Phys. Rev. B **29**, 5708(1984)

[41] S. Blakemore, *Semiconductor Statistics* (Pergamon, New York, 1962)

[42] Y. K. Hsu, C. S. Chang, and W. F. Hsieh, Jpn. J. Appl. Phys. **42**, 4222(2003)

[43] S. S. Ishchenko and A. A. Klimov, Phys. Solid State **40**, 55(1998)

[44] Ph. Schmid, IL Nuovo Cimento **21B**, 258(1974)

[45] H. Brooks, *Advances in Electronics and Electron Physics* (Academic, New York, 1995)

[46] C. Erginsoy, Phys. Rev. **79**, 1013(1950)

[47] P. C. Leung, G. Andermann, W. G. Spitzer, and C. A. Mead, J. Phys. Chem. Solids **27**, 849(1966)

[48] D. V. Lang, J. Appl. Phys. **45**, 3023(1974)

[49] N. B. Singh, D. R. Suhre, W. Rosch, M. Marable, R. Meyer, N. C. Fernelius, F. K. Hopkins, D. E. Zelmon, and R. Narayanan, J. Crystal Growth **198/199**, 588(1999)

[50] D. R. Suhre, N. B. Singh, V. Balakrishna, N. C. Fernelius, and F. K. Hopkins, Opt. Lett. **22**, 775(1997)

[51] M. Sato, T. Hatanaka, S. Izumi, T. Taniuchi, and H. Ito, Appl. Opt. **38**, 2559(1999)

[52] T. Hatanaka, K. Nakamura, T. Taniuchi, and H. Ito, Opt. Lett. **25**, 651(2000)

[53] S. J. Brosnan and R. L. Byer, IEEE J. Quantum Electron. **QE-15**, 415(1979)

[54] G. B. Abdullaev, L. A. Kulevskii, A. M. Prokhorov, A. D. Savelev, E. Yu. Salaev, and V. V. Smirnov, JETP Lett. **16**, 130(1972)

[55] K. L. Vodopyanov and L. A. Kuleskii, Opt. Commun. **118**, 375(1995)

[56] T. Dahinten, U. Plodereder, A. Seilmeier, K. L. Vodopyannov, K. R. Allakhverdiev, and Z. A. Ibragimov, IEEE J. Quantum Electron. **QE-29**, 2245(1993)

[57] K. Finsterbusch, A. Bayer, and H. Zacharias, Appl. Phys. B **79**, 457(2004)

Publications List:

(A) 期刊論文

1. **Y.K. Hsu**, J.J. Wang, C.S. Chang, and S.C. Wang, 2002, "*Synthesis of Bulk Beta-FeSi₂ Crystal*", Japanese Journal of Applied Physics, Vol.41 (2002) pp.3854-3859.

2. S. Haidar, **Y.K. Hsu**, C.S.Chang, S.C. Wang, and H. Ito, "*Difference Frequency Mixing of Periodically Poled Lithium Niobate OPO Output Waves in GaSe Crystal*", Optical Engineering, Vol.41 (2002) pp.1932-1935.

3. **Y.K. Hsu**, C.S. Chang, and W.F. Hsieh,"*Photoluminescence study of GaSe doped with Er*", Japanese Journal of Applied Physics Vol.42, (2003) pp4222-4225.

4. S.H. Lee, **Y.K. Hsu**, H.C. Hsu, C.S. Chang, and W.F. Hsieh, "*Fabrication and Optical Property of GaSe Thin Films Growth by Pulsed Laser Deposition*", Japanese Journal of Applied Physics Vol.42 (2003) pp.5217-5221.

5. **Y.K. Hsu**, W.C. Huang, and C.S. Chang, "*Electrical properties of GaSe doped with Er*", Journal of Applied Physics Vol.96, (2004) pp1563-1567.

(B) 研討會論文

1. S. Haidar, T. Usami, **Y.K. Hsu**, C.S. Chang, S.C.Wang, and H. Ito, "*Difference frequency mixing of periodically poled lithium niobate (PPLN) OPO output waves in GaSe crystal*", Technical Digest. Conference on Lasers and Electro-Optics, 2002.

2. C.Y. Lee, C.H. Lin, **Y.K. Hsu**, C.S. Chang, W.F. Hsieh, "Nonlinear optical characteristics of GaSe crystal by Z-scan measurement" Optics and Photonics Taiwan 02, Taipei, Taiwan, 2002.

3. M.D. Lee, H.C. Hsu, **Y.K. Hsu**, C.S. Chang, and W.F. Hsieh "*Van der Waals epitaxy of GaSe thin film on hydrogen-terminated Si(111) surfaces by pulsed laser deposition*", Annual Meeting of ROC Physics Society, Taiwan, 2002.

4. C.Y. Lu, **Y.K. Hsu**, and W.F. Hsieh, "*Investigation of electro-optical semiconductor GaSe on different substrates by pulsed laser deposition*", Annual Meeting of ROC Physics Society, Taiwan, 2003.

5. P.J. Jiang, **Y.K. Hsu**, and C.S. Chang "*Mid-infrared generation by difference frequency conversion in the GaSe crystal doped with Er and In*" Annual Meeting of ROC Physics Society, Taiwan, 2004.

6. Y.H. Lin, J.H. Lin, **Y.K. Hsu**, C.S. Chang, W.F. Hsieh "*Femtosecond Z-scan measurement of GaSe*" Optics and Photonics Taiwan 04, Taiwan, 2004.

候選人簡歷

♦ 姓名：徐裕奎

性別：男

出生年月日：民國 64 年 7 月 12 日

籍貫：台灣新竹

♦ 學歷：

私立東海大學物理學系學士　　　　　　　　　　　　(82.9~86.6)

國立交通大學光電工程研究所碩士　　　　　　　　　(86.9~88.6)

國立交通大學光電工程研究所博士　　　　　　　　　(88.9~94.6)

♦ 經歷：

2002 年 12 月至日本 Tohoku 大學與 H．Ito 教授實驗室從事非線性
光學實驗研究合作

♦ 博士題目：

硒化鎵晶體摻鉺特性及其應用在產生中紅外光源之研究

***The Study of the Characteristics of Er:GaSe Crystal and Application
to IR Source Generation***